Table 1
Clinical characteristics of patients.

Patient no.	Age (years)	Gender	Diagnosis (DSM-IV)	Dose of sulpiride (mg)	Duration of illness (years)	PANSS			
						Positive	Negative	General	Total
1	32	M	295.30	1200	15	16	21	30	67
2	45	F	295.30	600	28	25	26	49	100
3	47	M	295.30	1200	8	18	23	44	85
4	47	M	295.30	1000	25	23	26	47	96
5	52	M	295.10	1200	5	13	33	46	92
6	56	M	295.60	600	29	20	43	59	122
Mean ± SD	46.5 ± 8.2			966.7 ± 294.4	18.3 ± 10.5	19.2 ± 4.4	28.7 ± 8.1	45.8 ± 9.4	93.7 ± 18.1

DSM-IV, Diagnostic and Statistical Manual of Mental Disorders, 4th edition; PANSS, Positive and Negative Scale for Schizophrenia; M, Male; F, Female.

met the criteria of the Diagnostic and Statistical Manual of Mental Disorders 4th edition (DSM-IV) for diagnosis of schizophrenia. The diagnosis was assessed by Structured Clinical Interview for DSM-IV by three psychiatrists. The patients underwent general medical and laboratory evaluation. Organic brain disease was ruled out by CT, T1-weighted magnetic resonance (MR) images, and electroencephalogram.

Prior to this study, they had been prescribed antipsychotics during the periods indicated as 'duration of illness' in Table 1. In chlorpromazine equivalents, daily doses ranged from 200 mg to 606 mg and mean dose was 384 ± 139 mg/day (Inagaki and Inada 2006).

In all patients, the previously used antipsychotic drugs were changed to sulpiride, a selective dopamine D_2/D_3 receptor antagonist without affinity to dopamine D_1 receptor. PET scans were performed after a washout period of at least three weeks after changing to sulpiride. Sulpiride was maintained at the same dosage during the washout period. Because of extrapyramidal side effects, two patients were administered a relatively low dose of sulpiride (600 mg), although there had been no exacerbation of their psychic symptoms. All patients underwent clinical ratings of their psychopathology using the positive and negative syndrome scale (PANSS; Kay et al. 1987), and the following cognitive function tests: Wisconsin Card Sorting Test (Heaton 1981) to evaluate executive function, Stroop test (Cohen and Servan-Schreiber 1992) and *n*-back tasks (2-back minus 0-back using letters as stimulus; Cohen et al. 1994; Owen et al. 2005) to evaluate working memory.

The healthy control sample consisted of 6 females and 6 males, age-matched at 42.8 ± 8.5 years. Based on unstructured psychiatric screening interviews, none had a history of neurological or psychiatric illness. Organic brain disease was ruled out by T1-weighted MRI.

The study was approved by the Ethics and Radiation Safety Committees of the National Institute of Radiological Sciences, Chiba, Japan. After providing a complete explanation of the study, written informed consent was obtained from all subjects.

PET and MRI procedures

All patients except patient #6 (Table 1) underwent both PET scans using [^{11}C]NNC112 and [^{11}C]SCH23390 on the same day. Patient #6 and twelve healthy controls underwent each of the PET scans with [^{11}C]NNC112 and [^{11}C]SCH23390 within several days. The PET system ECAT EXACT HR+ (CT1-Siemens, Knoxville, TN) was used for all PET studies. The system provides 63 planes with a 15.5 cm axial field of view. After a transmission scan with a ^{68}Ge–^{68}Ga source, a bolus of [^{11}C]NNC112 or [^{11}C]SCH23390 was rapidly injected into the antecubital vein with a 20-ml saline flush. Injected radioactivity and specific radioactivity were 220.5 ± 9.25 MBq and 140.0 ± 64.1 GBq/μmol for patients in the [^{11}C]NNC112 studies, 215.0 ± 14.1 MBq and 152.5 ± 50.6 GBq/μmol for controls in the [^{11}C]NNC112 studies, 200.2 ± 15.9 MBq and 59.7 ± 15.5 GBq/μmol for patients in the [^{11}C]SCH23390 studies, and 220.5 ± 18.1 MBq and 68.6 ± 11.0 GBq/μmol for controls in the [^{11}C]SCH23390 studies, respectively.

Radioactivity in the brain was measured by a series of scans for 90 min for [^{11}C]NNC112 or 60 min for [^{11}C]SCH23390, starting immediately after the injection. During image acquisition, the subjects were instructed to lie quietly with their eyes closed and earplugs in place. Image reconstruction was performed with a Hanning filter with a cut-off frequency of 0.4, a value experientially determined for the purpose of noise reduction, resulting in a final spatial resolution of 7.5 mm FWHM (full width at half maximum).

T1-weighted MR images were acquired on Philips Gyroscan NT, 1.5 T (Philips Medical Systems, Best, The Netherlands). Scan parameters were 1-mm-thick 3D images with a transverse plane (repetition time, TR/echo time, TE 21/9.2 ms, flip angle 30°, matrix 256 × 256, field of view (FOV) 256 × 256), yielding 196 contiguous slices of the head.

PET data analysis

Regions of interest (ROIs) were manually drawn on the transverse slices from each subject's PET summation images referred from MRI images coregistered to the reconstructed PET images. ROIs were set to cover 3 adjacent slices for the striatum including both the caudate nucleus and the putamen, anterior cingulate, cerebellum, temporal cortex and frontal cortex including the superior frontal gyrus, middle frontal gyrus, and inferior frontal gyrus, which roughly corresponds to dorsolateral prefrontal cortex. The sets of ROIs for each section were transferred to the corresponding PET images, and time–activity curves (TACs) were obtained. The TACs of each region were analyzed using a simplified reference tissue model in a least-squares manner, in which the cerebellum was used as reference tissue (Lammertsma and Hume 1996). This procedure produced the binding potential (BP_{ND}; Innis et al. 2007) value.

Statistical analysis

Statistical analysis of the regional BP_{ND} obtained from patients with schizophrenia and healthy control subjects was performed using one-way analysis of covariance (one-way ANCOVA) with age as covariate using SPSS for Windows 16.0.2J (SPSS Inc, Chicago, Illinois, USA 2008), and post hoc Bonferroni correction was used for multiple comparisons. p value $< 0.05/4 = 0.0125$ was considered significant.

Results

Table 1 lists the clinical profiles of the patients. The average duration of illness after schizophrenia diagnosis was 18.3 years. Scores of the two cognitive functional tests are shown in Table 2, and significant group effects were found in each cognitive function test. Because four patients, #2, #3, #5 and #6, were not able to do *n*-back task (2 back), results were not shown in Table 2.

Significant correlations between BP_{ND} and age were observed in patients with [^{11}C]NNC112 (frontal cortex, $r = -0.924$, $p = 0.004$; striatum, $r = -0.981$, $p = 0.001$), controls with [^{11}C]NNC112 (striatum, $r = -0.886$, $p < 0.001$) and controls with [^{11}C]SCH23390 (frontal cortex, $r = -0.757$, $p = 0.004$; striatum, $r = -0.700$, $p = 0.011$). Trend

Table 2
Cognitive task scores of patients.

Patient no.	W-CST			Stroop test	
	Category	PEN	DMS	Error	Time score
1	6	0	0	0	17.4
2	2	9	5	11	46.6
3	1	7	3	1	7.4
4	5	1	1	0	5.4
5	2	14	0	2	68
6	Incapable	Incapable	Incapable	2	75
Mean ± SD	3.2 ± 2.2	6.2 ± 5.8	1.8 ± 2.2	2.7 ± 4.2	36.6 ± 30.8
Controls					
Mean ± SD	4.7 ± 1.6	1.4 ± 2.0	0.8 ± 1.4	0.8 ± 1.2	5.6 ± 4.0

W-CST, Wisconsin card sorting test; PEN, errors of nelson; DMS, difficulty in maintaining set.

level correlations were observed in other regions and patients with [^{11}C]SCH23390.

All BP_{ND} values of both ligands are shown in Fig. 1 and summarized in Table 3. ANCOVA with age as covariate ($df = 1,15$) of BP_{ND} values of all ROIs revealed that the patient group showed significantly lower BP_{ND} value compared with the control group in both ligands ([^{11}C]NNC112: temporal cortex, $F = 26.24$, $p < 0.001$; striatum, $F = 60.08$, $p < 0.001$; anterior cingulate cortex, $F = 9.14$, $p = 0.009$; frontal cortex, $F = 42.96$, $p < 0.001$, [^{11}C]SCH23390: temporal cortex, $F = 34.68$, $p < 0.001$; striatum, $F = 25.46$, $p < 0.001$; anterior cingulate cortex, $F = 8.91$, $p = 0.009$; frontal cortex, $F = 37.60$, $p < 0.001$). There was significant correlation between average BP values of [^{11}C]NNC112 weighted by ROI size and that of [^{11}C]SCH23390 ($r = 0.859$; $BP_{NNC} = 0.613\ BP_{SCH} + 0.0414$).

There was no significant correlation between BP_{ND} values and doses of antipsychotic drugs and between BP_{ND} values and PANSS scores for positive symptom, negative symptom, general symptom and total score in any of the brain regions.

Discussion

Both [^{11}C]NNC112 and [^{11}C]SCH23390 bindings in the striatum and cortical regions of patients with schizophrenia in severe residual phase were significantly lower compared with healthy controls. In previous PET studies of patients with schizophrenia who were antipsychotics-naïve or -free, BP of [^{11}C]SCH23390 was decreased (Okubo et al. 1997) or unchanged (Karlsson et al. 2002), and was increased when measured by [^{11}C]NNC112 (Abi-Dargham et al. 2002). Several differences in those studies have been discussed, including those regarding duration of illness, medications, race, severity of symptoms and radioligands. Guo et al. (2003) reported different characteristics of in vivo binding of the two radioligands in rat brain, increased [^{11}C]NNC112 binding and decreased [^{3}H]SCH23390 binding, following subchronic dopamine depletion with reserpine. But the inconsistent results cannot be explained solely by the difference of radiotracers, and demographics of patients might have been contributing factors.

Although [^{11}C]SCH23390 and [^{11}C]NNC112 are selective radioligands for dopamine D_1 receptor, both ligands have some affinity for 5-

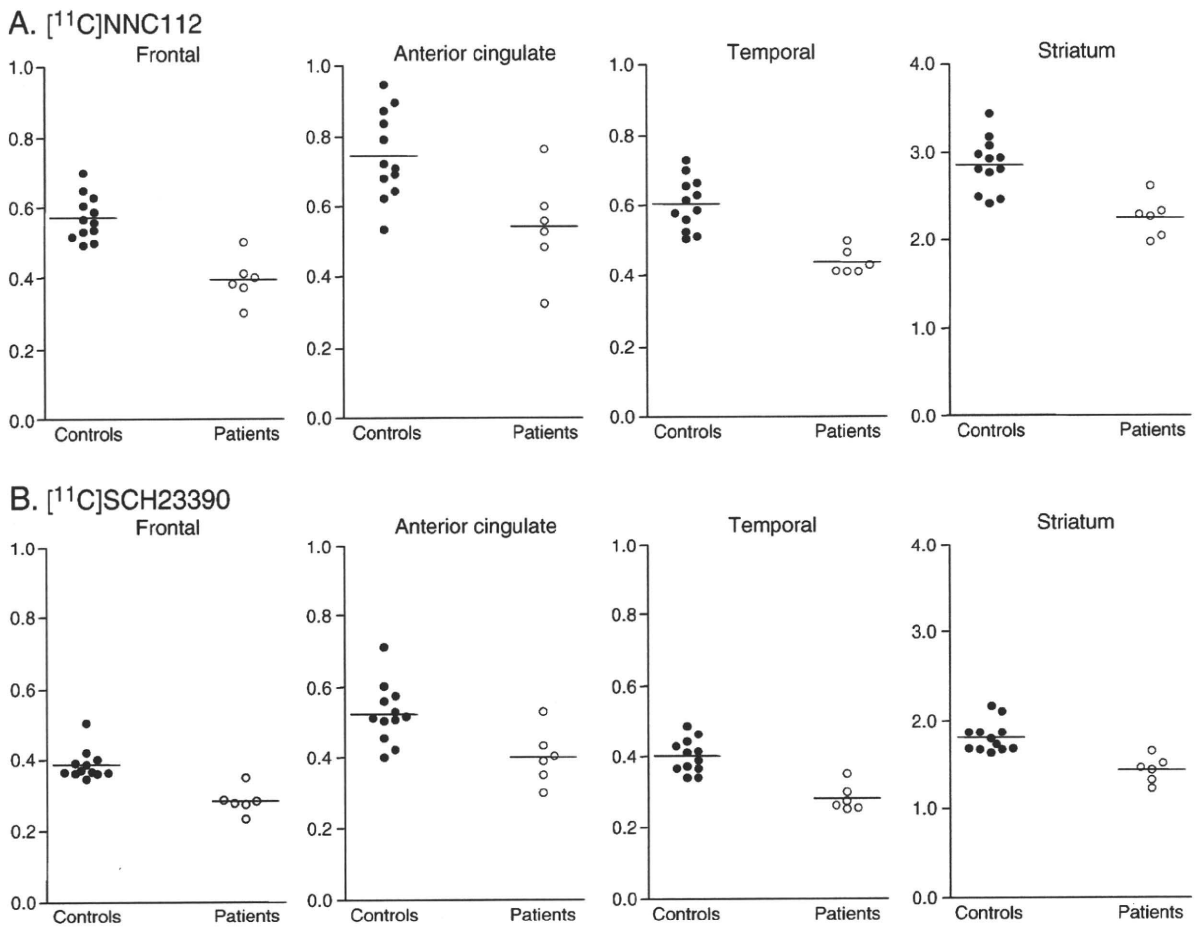

Fig. 1. BP_{ND} values of all subjects in both ligands [^{11}C] NNC112 and [^{11}C]SCH23390. Filled circles represent controls and open circles represent patients. A. BP_{ND} measured by [^{11}C] NNC112; B. BP_{ND} measured by [^{11}C]SCH23390. The horizontal line represents the group mean. In all ROIs, statistically significant differences were observed between patients with schizophrenia and healthy controls (one-way ANCOVA with age as covariate, $p < 0.0125 = 0.05/4$).

Table 3
[^{11}C] NNC112 and [^{11}C]SCH23390 binding potential.

Region	[^{11}C]NNC112				[^{11}C]SCH23390			
	Controls ($n=12$)	Patients ($n=6$)	p value	Reduction (%)	Controls ($n=12$)	Patients ($n=6$)	p value	Reduction (%)
Frontal cortex	0.57 ± 0.064	0.39 ± 0.065	<0.001*	31.2	0.39 ± 0.043	0.28 ± 0.037	<0.001*	26.7
Anterior cingulate	0.75 ± 0.12	0.54 ± 0.14	0.009*	27.2	0.53 ± 0.083	0.40 ± 0.079	0.009*	23.5
Temporal cortex	0.61 ± 0.074	0.44 ± 0.037	<0.001*	27.7	0.40 ± 0.048	0.28 ± 0.038	<0.001*	29.9
Striatum	2.85 ± 0.31	2.25 ± 0.23	<0.001*	21.4	1.83 ± 0.18	1.45 ± 0.15	<0.001*	20.9

Data are mean ± SD.
* $p<0.0125$ (= 0.05/4, Bonferroni corrected) ANCOVA with age as covariate ($df=1,15$).

HT_{2A} receptor (Slifstein et al. 2007). However, Okubo et al. (2000) reported no difference in binding in the prefrontal cortex using [^{11}C]N-methylspiperone as ligand for 5-HT2 receptor in the same schizophrenia patients who showed lower binding with [^{11}C]SCH23390 (Okubo et al. 1997) and a non-significant trend towards decreased binding. In this study, all patients were medicated with only sulpiride as antipsychotic drug. Sulpiride is a selective dopamine D_2 antagonist and has negligible affinity to dopamine D_1 receptor in vivo (Farde et al. 1989). All antipsychotics of the patients were changed to sulpiride. Even though sulpiride had no direct affinity to dopamine D_1 receptor, these patients had been receiving long-term chronic antipsychotic treatment. Several studies of primates have reported that chronic administration of dopamine D_2 receptor antagonist decreased the density of dopamine D_1 receptor (Lidow and Goldman-Rakic 1994; Lidow et al. 1997), although one animal study has reported that there was no influence of chronic medication on dopamine D_1 receptor density (Sanci et al. 2002). Hirvonen et al. (2006) reported a widespread reduction of D_1 receptor binding in the brain in patients with schizophrenia, which was associated with antipsychotic medication dose. However, we did not find a correlation between them, possibly due to a lack of variance in antipsychotic dose.

The patients in this study were in a very severe residual phase according to the deficits in the cognitive test scores (Table 2) and the high total scores of PANSS despite the low positive symptom scores (Table 1). Some studies have reported regional structural brain abnormalities of gray matter in the striatum and extrastriatal regions of schizophrenia patients with chronic antipsychotic treatment (Jernigan et al. 1991; Tamagaki et al. 2005). In this study, since we confirmed that there was no significant difference between the volume of each ROI in patients and that of controls, we measured the gray matter volume ratio in each ROI. The results revealed no significant difference between the gray matter volume in patients and that of controls in each ROI (data not shown). The values of reduction in BP_{ND} shown by percentage (Table 3) seemed considerably larger than the reduction of gray matter. However, the effect of brain gray matter reduction cannot also be ruled out.

Our results indicated lower dopamine D_1 receptor binding in schizophrenia patients with chronic antipsychotic treatment measured by different radioligands, [^{11}C]NNC112 and [^{11}C]SCH23390. However, as the small sample size was a distinct limitation of this study, a larger study population will be necessary to more definitively examine the relation between dopamine D_1 receptor binding and factors such as duration of illness and severity of symptoms.

Conflict of interest statement

There are no conflicts of interests.

Acknowledgements

This study was supported by a consignment expense for the Molecular Imaging Program on "Research Base for PET Diagnosis" from the Ministry of Education, Culture, Sports, Science and Technology (MEXT), Japanese Government. The sponsors of the study had no role in the study design, collection, analysis, and interpretation of data, in the writing of the report, or in the decision to submit the paper for publication.

We thank Mr. Takahiro Shiraishi and Mr. Akira Ando for their assistance in performing the PET experiments at the National Institute of Radiological Sciences. We also thank Ms. Yoshiko Fukushima of the National Institute of Radiological Sciences for her help as clinical research coordinator, and Miho Shidahara is acknowledged for her valuable comments.

References

Abi-Dargham A, Mawlawi O, Lombardo I, Gil R, Martinez D, Huang Y, Hwang DR, Keilp J, Kochan L, Van Heertum R, Gorman JM, Laruelle M. Prefrontal dopamine D1 receptors and working memory in schizophrenia. The Journal of Neuroscience 22 (9), 3708–3719, 2002.

Cohen JD, Servan-Schreiber D. Context, cortex, and dopamine: a connectionist approach to behavior and biology in schizophrenia. Psychological Review 99, 45–77, 1992.

Cohen JD, Forman SD, Braver TS, Casey BJ, Servan-Schreiber D, Noll DC. Activation of the prefrontal cortex in a nonspatial working memory task with functional MRI. Human Brain Mapping 1, 293–304, 1994.

Czudek C, Reynolds G. Binding of [11C]SCH 23390 to post-mortem brain tissue in schizophrenia. British Journal of Pharmacology 93, 166P suppl, 1988.

Farde L, Wiesel FA, Nordström AL, Sedvall G. D1- and D2-dopamine receptor occupancy during treatment with conventional and atypical neuroleptics. Psychopharmacology (Berl) 99, S28–S31 Suppl, 1989.

Goldman-Rakic PS, Muly 3rd EC, Williams GV. D1 receptors in prefrontal cells and circuits. Brain Research Reviews 31 (2–3), 295–301, 2000.

Guo N, Hwang DR, Lo ES, Huang YY, Laruelle M, Abi-Dargham A. Dopamine depletion and in vivo binding of PET D1 receptor radioligands: implications for imaging studies in schizophrenia. Neuropsychopharmacology 28 (9), 1703–1711, 2003.

Heaton RK. A Manual for the Wisconsin Card Sorting Test. Psychological Assessment Resources, Odessa, FL, 1981.

Hess EJ, Bracha HS, Kleinman JE, Creese I. Dopamine receptor subtype imbalance in schizophrenia. Life Sciences 40 (15), 1487–1497, 1987.

Hirvonen J, van Erp TG, Huttunen J, Aalto S, Någren K, Huttunen M, Lönnqvist J, Kaprio J, Cannon TD, Hietala J. Brain dopamine D1 receptors in twins discordant for schizophrenia. The American Journal of Psychiatry 163 (10), 1747–1753, 2006.

Inagaki A, Inada T. Dose equivalence of psychotropic drugs: 2006-version. Rinsyou Seisihn Yakuri (Clinical Psychopharmachology) 9, 1443–1447 in Japanese, 2006.

Innis RB, Cunningham VJ, Delforge J, Fujita M, Gjedde A, Gunn RN, Holden J, Houle S, Huang SC, Ichise M, Iida H, Ito H, Kimura Y, Koeppe RA, Knudsen GM, Knuuti J, Lammertsma AA, Laruelle M, Logan J, Maguire RP, Mintun MA, Morris ED, Parsey R, Price JC, Slifstein M, Sossi V, Suhara T, Votaw JR, Wong DF, Carson RE. Consensus nomenclature for in vivo imaging of reversibly binding radioligands. Journal of Cerebral Blood Flow and Metabolism 27 (9), 1533–1539, 2007.

Jernigan TL, Zisook S, Heaton RK, Moranville JT, Hesselink JR, Braff DL. Magnetic resonance imaging abnormalities in lenticular nuclei and cerebral cortex in schizophrenia. Archives General Psychiatry 48 (10), 881–890, 1991.

Karlsson P, Farde L, Halldin C, Sedvall G. PET study of D1 dopamine receptor binding in neuroleptic-naïve patients with schizophrenia. The American Journal of Psychiatry 159 (5), 761–767, 2002.

Kay SR, Fiszbein A, Opler LA. The positive and negative syndrome scale (PANSS) for schizophrenia. Schizophrenia Bulletin 13 (2), 261–276, 1987.

Knable MB, Hyde TM, Herman MM, Carter JM, Bigelow L, Kleinman JE. Quantitative autoradiography of dopamine-D1 receptors, D2 receptors, and dopamine uptake sites in postmortem striatal specimens from schizophrenic patients. Biological Psychiatry 36 (12), 827–835, 1994.

Lammertsma AA, Hume SP. Simplified reference tissue model for PET receptor studies. Neuroimage 4 (3 Pt 1), 153–158, 1996.

Lidow MS, Goldman-Rakic PS. A common action of clozapine, haloperidol, and remoxipride on D1- and D2-dopaminergic receptors in the primate cerebral cortex. Proceedings of the National Academy Sciences of the U.S.A. 91, 4353–4356, 1994.

Lidow MS, Elsworth JD, Goldman-Rakic PS. Down-regulation of the D1 and D5 dopamine receptors in the primate prefrontal cortex by chronic treatment with antipsychotic drugs. The Journal of Pharmacology and Experimental Therapeutics 281 (1), 597–603, 1997.

Lidow MS, Williams GV, Goldman-Rakic PS. The cerebral cortex: a case for a common site of action of antipsychotics. Trends in Pharmacological Sciences 19 (4), 136–140, 1998.

Okubo Y, Suhara T, Suzuki K, Kobayashi K, Inoue O, Terasaki O, Someya Y, Sassa T, Sudo Y, Matsushima E, Iyo M, Tateno Y, Toru M. Decreased prefrontal dopamine D1 receptors in schizophrenia revealed by PET. Nature 385 (6617), 634–636, 1997.

Okubo Y, Suhara T, Suzuki K, Kobayashi K, Inoue O, Terasaki O, Someya Y, Sassa T, Sudo Y, Matsushima E, Iyo M, Tateno Y, Toru M. Serotonin 5-HT2 receptors in schizophrenic patients studied by positron emission tomography. Life Sciences 66 (25), 2455–2464, 2000.

Owen AM, McMillan KM, Laird AR, Bullmore E. N-back working memory paradigm: a meta-analysis of normative functional neuroimaging studies. Human Brain Mapping 25 (1), 46–59, 2005.

Sanci V, Houle S, DaSilva JN. No change in dopamine D1 receptor in vivo binding in rats after sub-chronic haloperidol treatment. Canadian Journal of Physiology and Pharmacology 80 (1), 36–41, 2002.

Sawaguchi T, Goldman-Rakic PS. D1 dopamine receptors in prefrontal cortex: involvement in working memory. Science 251 (4996), 947–950, 1991.

Schultz SK, Andreasen NC. Schizophrenia. Lancet 353 (9162), 1425–1430, 1999.

Seeman P, Bzowej NH, Guan HC, Bergeron C, Reynolds GP, Bird ED, Riederer P, Jellinger K, Tourtellotte WW. Human brain D1 and D2 dopamine receptors in schizophrenia, Alzheimer's, Parkinson's, and Huntington's diseases. Neuropsychopharmacology 1 (1), 5–15, 1987.

Slifstein M, Kegeles LS, Gonzales R, Frankle WG, Xu X, Laruelle M, Abi-Dargham A. [^{11}C]NNC 112 selectivity for dopamine D1 and serotonin 5-HT(2A) receptors: a PET study in healthy human subjects. Journal of Cerebral Blood Flow and Metabolism 27 (10), 1733–1741, 2007.

Tamagaki C, Sedvall GC, Jönsson EG, Okugawa G, Hall H, Pauli S, Agartz I. Altered white matter/gray matter proportions in the striatum of patients with schizophrenia: a volumetric MRI study. The American Journal of Psychiatry 162 (12), 2315–2321, 2005.

International Journal of Neuropsychopharmacology (2011), **14**, 83–89. © CINP 2010
doi:10.1017/S1461145710001148

ARTICLE

THEMATIC SECTION
New Developments in Schizophrenia Research

CINP

Effect of risperidone on high-affinity state of dopamine D_2 receptors: a PET study with agonist ligand [^{11}C](R)-2-CH_3O-N-n-propylnorapomorphine

Fumitoshi Kodaka[1,2], Hiroshi Ito[1], Harumasa Takano[1], Hidehiko Takahashi[1], Ryosuke Arakawa[1], Michie Miyoshi[1], Masaki Okumura[1], Tatsui Otsuka[1], Kazuhiko Nakayama[2], Christer Halldin[3], Lars Farde[3] and Tetsuya Suhara[1]

[1] *Clinical Neuroimaging Team, Molecular Neuroimaging Group, Molecular Imaging Center, National Institute of Radiological Sciences, Chiba, Japan*

[2] *Department of Psychiatry, Jikei University School of Medicine, Tokyo, Japan*

[3] *Department of Clinical Neuroscience, Karolinska Institutet, Stockholm, Sweden*

Abstract

The increased proportion of the high-affinity state of dopamine $D_{2/3}$ receptors ($D_{2,high}$) is assumed to correlate with dopamine hypersensitivity, implying a relationship with psychotic symptoms observed in psychiatric disorders such as schizophrenia. [^{11}C](R)-2-CH_3O-N-n-propylnorapomorphine ([^{11}C]MNPA), which has an agonistic property to dopamine D_2 receptors (D_2Rs), is expected to bind preferentially to $D_{2,high}$. The occupancy of dopamine D_2Rs by antagonists to receptors has not been investigated using [^{11}C]MNPA. We compared dopamine D_2R occupancies by risperidone, an antagonist to receptors, between [^{11}C]MNPA and [^{11}C]raclopride to confirm whether risperidone occupies $D_{2,high}$ and $D_{2,low}$ at almost identical proportions. PET studies were performed on 11 healthy men under resting condition and following oral administration of a single dose of risperidone (0.5–2.0 mg). Striatal receptor occupancy for each radioligand was calculated. The relationship between dose or plasma concentration of risperidone and dopamine D_2R occupancy was calculated. Striatal dopamine D_2R occupancies measured with [^{11}C]MNPA and [^{11}C]raclopride were 22–65% and 24–69%, respectively. In the striatum, ED_{50} values measured with [^{11}C]MNPA and [^{11}C]raclopride were 0.98 and 1.03 mg, respectively. The striatal ED_{50} values as calculated from plasma concentration were 9.15 ng/ml and 8.01 ng/ml, respectively. Almost identical occupancies and ED_{50} values were observed between the two radioligands, indicating that risperidone bound to $D_{2,high}$ and $D_{2,low}$ at almost identical proportions in a dose-dependent manner.

Received 7 May 2010; Reviewed 1 June 2010; Revised 15 August 2010; Accepted 23 August 2010; First published online 22 September 2010

Key words: Binding potential, dopamine D_2 receptor, receptor occupancy, risperidone, [^{11}C]MNPA.

Introduction

The dopaminergic neurotransmission system is of central interest in schizophrenia, and dopamine D_2 receptors (D_2Rs) are the main target in the treatment with antipsychotics (Seeman *et al.* 1975). Early *in-vitro* studies reported that dopamine D_2Rs have two interconvertible affinity states for endogenous dopamine, referred to as high-affinity ($D_{2,high}$) and low-affinity ($D_{2,low}$) states (De Lean *et al.* 1982; George *et al.* 1985; Richfield *et al.* 1989; Sibley *et al.* 1982). D_2R antagonists are reported to have equal affinity to both states of receptors, while endogenous dopamine preferentially binds to $D_{2,high}$ (Seneca *et al.* 2006). The increased proportion of $D_{2,high}$ is assumed to correlate with dopamine hypersensitivity, implying a relationship with psychotic symptoms observed in psychiatric disorders such as schizophrenia (Seeman *et al.* 2005).

[^{11}C]raclopride, an antagonist radioligand for dopamine D_2Rs, has been used to measure striatal

Address for correspondence: H. Ito, M. D., Ph.D., Clinical Neuroimaging Team, Molecular Neuroimaging Group Molecular Imaging Center, National Institute of Radiological Sciences, 4-9-1 Anagawa, Inage-ku, Chiba 263-8555, Japan.
Tel.: (+81) 43-206-4702 *Fax*: (+81) 43-253-0396
Email: hito@nirs.go.jp

dopamine D_2R binding with positron emission tomography (PET). [^{11}C]raclopride is thought to bind to both $D_{2,high}$ and $D_{2,low}$. Recently, several agonist radioligands for dopamine D_2Rs that are thought to bind preferentially to $D_{2,high}$ were developed, i.e. (−)-N-[^{11}C]propyl-norapomorphine ([^{11}C]NPA; Hwang *et al.* 2000), [^{11}]C(+)-4-propyl-3,4,4a,5,6,10b-hexahydro-2H-naphtho[1,2-b][1,4]oxazin-9-ol ([^{11}C]PHNO; Wilson *et al.* 2005), and [^{11}C](R)-2-CH3O-N-n-propylnorapomorphine ([^{11}C]MNPA). [^{11}C]MNPA has high selectivity and affinity to dopamine D_2Rs (IC_{50}: 1.02 nM, K_i: 0.17 nM; Gao *et al.* 1990; Neumeyer *et al.* 1990) and is believed to bind preferentially to the high-affinity state of dopamine $D_{2/3}Rs$.

The receptor occupancy for endogenous dopamine and dopamine agonists using [^{11}C]MNPA and [^{11}C]raclopride has been studied (Finnema *et al.* 2009; Seneca *et al.* 2006), but occupancy by dopamine antagonists was not fully investigated using [^{11}C]MNPA (Finnema *et al.* 2005). Most antipsychotic drugs are antagonists to dopamine D_2Rs, and the antipsychotic effects of such drugs have been considered to be mediated by blockade of dopamine D_2Rs. The degree of blockade can be evaluated by the occupancy of dopamine D_2Rs using PET. Because dopamine D_2R antagonists bind to both $D_{2,high}$ and $D_{2,low}$, occupancies of dopamine D_2Rs by antagonist antipsychotic drugs measured with [^{11}C]raclopride and [^{11}C]MNPA are expected to be the same.

In the present study, we measured dopamine D_2R occupancies by administration of a single dose of the antipsychotic risperidone as a dopamine D_2R antagonist using both [^{11}C]raclopride and [^{11}C]MNPA in healthy subjects. The dose–occupancy curves and the ED_{50} values in the putamen and caudate nuclei were compared between [^{11}C]raclopride and [^{11}C]MNPA.

Materials and methods

Subjects

Eleven healthy male volunteers (age range 21–39 yr, mean ± S.D. 27 ± 7.4yr) were recruited and written informed consent was obtained. They were healthy according to T1- and T2-weighted magnetic resonance (MR) imaging (Philips Medical Systems, The Netherlands) and blood (blood cell count, aspartate aminotransferase, alanine aminotransferase, lactate dehydrogenase, gamma glutamyltransferase, creatine kinase, serum sodium, potassium, chlorine, blood urea nitrogen, serum creatinine, blood sugar) and urine screening tests. None had a history of psychiatric or neurological disorders, and they were free of physical disease. They had no history of current or previous drug abuse. The subjects were assigned to one of three groups according to risperidone dose: 0.5 mg ($n=5$), 1.0 mg ($n=3$), 2.0 mg ($n=3$). This study protocol was approved by the Ethics and Radiation Safety Committees of the National Institute of Radiological Science, Chiba, Japan.

PET procedures

All PET data were obtained with a Siemens ECAT Exact HR+ system, which provides 63 sections with an axial field of view of 15.5 cm (Brix *et al.* 1997). The intrinsic spatial resolution was 4.3 mm in-plane and 4.2 mm full-width at half-maximum (FWHM) axially. With a Hanning filter (cut-off frequency 0.4 cycle/pixel), the reconstructed in-plane resolution was 7.5 mm FWHM. Imaging data were acquired in 3D mode. Scatter correction was performed (Watson *et al.* 1996). A thermoplastic head fixation device was used to minimize head movement during PET scanning. A 10-min transmission scan using a ^{68}Ge–^{68}Ge line source was performed for attenuation correction.

PET studies were performed under resting condition (baseline study) and oral administration of risperidone (drug challenge study) on separate days. The average interval between the two studies was 8.3 ± 2.8 d. After intravenous rapid bolus injection of [^{11}C]raclopride, dynamic PET scanning was performed for 60 min. One hour after the end of [^{11}C]raclopride PET measurement, dynamic PET scanning was performed for 90 min after intravenous rapid bolus injection of [^{11}C]MNPA. The frame sequence comprised nine 20-s frames, five 60-s frames, four 120-s frames, eleven 240-s frames and six 300-s frames for [^{11}C]-MNPA, and twelve 20-s frames, sixteen 60-s frames and ten 240-s frames for [^{11}C]raclopride. Injected radioactivities for [^{11}C]MNPA and [^{11}C]raclopride under baseline conditions were 208–248 MBq and 207–241 MBq, respectively, and under drug challenge 214–235 MBq and 182–232 MBq, respectively, for [^{11}C]MNPA and [^{11}C]raclopride. The specific radioactivities for [^{11}C]MNPA and [^{11}C]raclopride under baseline conditions were 148–429 GBq/μmol and 222–736 GBq/μmol, respectively, and under drug challenge 103–411 GBq/μmol and 211–545 GBq/μmol, respectively.

Measurement of plasma concentration of risperidone

In the drug challenge study, 0.5–2 mg risperidone was orally administered 2 h prior to the start of PET scanning with [^{11}C]raclopride. To determine the plasma concentration of risperidone and its active metabolite

(9-hydroxy-risperidone), venous blood samples were drawn at 10–15 min before, and at 1 h, 2 h, 3 h, 4 h, 5.5 and 7 h after its oral administration.

The series of blood samples of each subject were collected in heparinized tubes and centrifuged for 10 min at 3000 rpm. All plasma samples were stored at −20 °C. The plasma concentrations of risperidone and 9-hydroxy-risperidone were determined using the liquid chromatography coupled to mass spectrometry/mass spectrometry (LC–MS/MS) method with a target lower limit of quantification of 0.10 ng/ml (Johnson & Johnson Pharmaceutical Research and Development L. L. C., Belgium). Since risperidone and 9-hydroxy risperidone have similar binding profiles to neuroreceptors (Leysen *et al.* 1994), the sum of the plasma concentrations of risperidone and 9-hydroxy-risperidone was used as the plasma concentration of the antipsychotic drug (Ito *et al.* 2009*a*; Leysen *et al.* 1994).

MR imaging

MR images were acquired with a 1.5-T MR scanner (Philips Medical Systems, The Netherlands). 3D volumetric acquisition of a T1-weighted gradient echo sequence produced a gapless series of thin transverse sections (TE 9.2 ms, TR 21 ms, flip angle 30°, field of view 256 mm, acquisition matrix 256 × 256, slice thickness 1 mm).

Data analysis

All data analyses were performed with PMOD 3.0 software (PMOD Technologies, Switzerland). Volumes of interest (VOIs) were defined for the caudate head, putamen, dorsal striatum (caudate head and putamen) and cerebellar cortex. For accurate definition of each VOI, each MR image was co-registered to the corresponding summated PET image. VOIs were drawn manually on each summated PET image with reference to each co-registered MR image. Subsequently, the data of each VOI were applied to each dynamic PET image. In the present study, we applied VOIs obtained from individual PET space according to the previous quantitative study of [^{11}C]MNPA in humans (Otsuka *et al.* 2009). To obtain regional time–activity curves, regional radioactivity was calculated for each frame, corrected for decay, and plotted *vs.* time.

Dopamine D_2R binding was quantified using a three-parameter simplified reference tissue model (Lammertsma & Hume, 1996). The cerebellar cortex was used as reference tissue due to its negligible density of dopamine D_2Rs (Suhara *et al.* 1999). This model allows the estimation of binding potential (BP_{ND}). BP_{ND} was defined as a follows:

$$BP_{ND} = f_{ND} \times B_{max}/K_d, \quad (1)$$

where f_{ND} is the free fraction of radioligand in the non-displaceable tissue compartment, B_{max} the neuroreceptor density, and K_d the dissociation constant of radioligand to receptors (Innis *et al.* 2007). The dopamine D_2R occupancies by risperidone were calculated as follows:

$$\text{occupancy } (\%) = (BP_{base} - BP_{drug})/BP_{base} \times 100, \quad (2)$$

where BP_{base} is the BP_{ND} in the drug-free state, and BP_{drug} the BP_{ND} under administration of risperidone (Takano *et al.* 2004, 2006; Yasuno *et al.* 2001). The relationship between the dose or the plasma concentration of antipsychotic drug and dopamine D_2R occupancy can be expressed as follows:

$$\text{occupancy } (\%) = D/(D + ED_{50}) \times 100, \quad (3)$$

where D is the dose or the sum of the plasma concentrations of risperidone and 9-hydroxy-risperidone (Nyberg *et al.* 1999), and ED_{50} is the plasma concentration required to induce 50% occupancy. The maximal occupancy of D_2Rs was restricted to 100% to reflect the expected maximal occupancy. All the regression analyses were performed using Kaleida Graph 4.01 software (Synergy Software, USA). The regression line was fitted according to equation (3), with calculation of the ED_{50} values and regression coefficients for each radioligand. The mean plasma concentration values at the start and end of PET scanning were used for the calculation of ED_{50} values.

Results

Baseline BP_{ND} values of [^{11}C]MNPA were 0.84 ± 0.1 in the striatum, 0.67 ± 0.1 in the caudate nuclei and 0.93 ± 0.1 in the putamen. Baseline BP_{ND} values of [^{11}C]raclopride were 3.17 ± 0.4 in the striatum, 2.83 ± 0.4 in the caudate nuclei and 3.37 ± 0.4 in the putamen (Table 1).

The dopamine D_2R occupancies using [^{11}C]MNPA ranged from 22% to 66% for the striatum, 34–78% for the caudate nuclei, and 17–67% for the putamen in the three dose groups. Receptor occupancies using [^{11}C]raclopride ranged from 18% to 70% for the striatum, 22–72% for the caudate nuclei, and 17–69% for the putamen.

Significant positive correlations of dopamine D_2R occupancies between [^{11}C]raclopride and [^{11}C]MNPA were observed in the caudate nuclei and putamen (caudate nuclei: $r = 0.65$, $p = 0.04$; putamen: $r = 0.86$, $p = 0.01$).

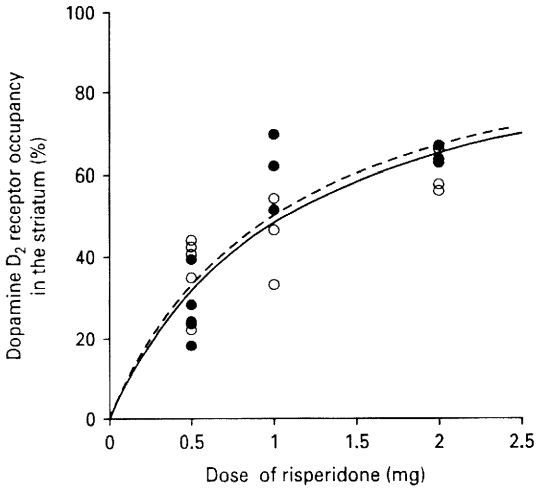

Fig. 1. The relationship between dopamine D_2 receptor occupancy in the striatum and risperidone dose. Open symbols (○) and solid curve (—) indicate receptor occupancy with [^{11}C]MNPA and its fitting curve, and solid symbols (●) and dashed curve (– – –) indicate receptor occupancy with [^{11}C]raclopride and its fitting curve, respectively. ED_{50} in the striatum was 1.08 and 1.00 mg for [^{11}C]MNPA and [^{11}C]raclopride, respectively.

The relationship between dopamine D_2R occupancy in the striatum and risperidone dose are shown in Fig. 1. These relationships are well described by equation (3) (striatum: $r=0.86$ and $r=0.68$; caudate nuclei: $r=0.86$ and $r=0.62$; putamen: $r=0.85$ and $r=0.78$ for [^{11}C]raclopride and [^{11}C]MNPA, respectively). The ED_{50} values calculated from [^{11}C]raclopride and [^{11}C]MNPA, respectively, were 1.00 mg ($r=0.86$) and 1.08 mg ($r=0.68$) in the striatum, 0.88 mg ($r=0.86$) and 0.80 mg ($r=0.62$) in the caudate nuclei, and 1.07 ($r=0.85$) mg and 1.00 mg ($r=0.78$) in the putamen.

The sum of plasma concentrations of risperidone and 9-hydroxy-risperidone during [^{11}C]raclopride and [^{11}C]MNPA studies, averaged between the start and end of each scanning, was 9.37 ± 4.89 ng/ml and 7.74 ± 3.91 ng/ml (mean ± S.D.), respectively. The relationship between dopamine D_2R occupancy in the striatum and the sum of plasma concentrations of risperidone and 9-hydroxy-risperidone are shown in Fig. 2. The ED_{50} values from the plasma concentration–occupancy curves with [^{11}C]raclopride and [^{11}C]MNPA, respectively, were 9.15 ng/ml ($r=0.91$) and 8.32 ng/ml ($r=0.36$) in the striatum, 8.00 ng/ml ($r=0.88$) and 6.12 ng/ml ($r=0.53$) in the caudate nuclei, and 9.75 ng/ml ($r=0.92$) and 7.70 ng/ml ($r=0.74$) in the putamen.

Table 1. The range of dopamine D_2 receptor binding potential values of [^{11}C]MNPA and [^{11}C]raclopride by dose of risperidone

	Baseline	0.5 mg	1.0 mg	2.0 mg
[^{11}C]MNPA				
Caudate head	0.40–0.81	0.32–0.49	0.21–0.33	0.16–0.39
Putamen	0.70–1.22	0.48–0.79	0.45–0.52	0.28–0.44
Dorsal striatum	0.84–0.13	0.44–0.65	0.40–0.40	0.26–0.41
[^{11}C]raclopride				
Caudate head	2.19–3.36	1.65–2.28	0.66–1.22	0.84–1.1
Putamen	2.56–4.11	2.37–2.86	1.00–1.44	1.03–1.44
Dorsal striatum	2.55–3.84	2.15–2.65	0.87–1.37	0.99–1.28

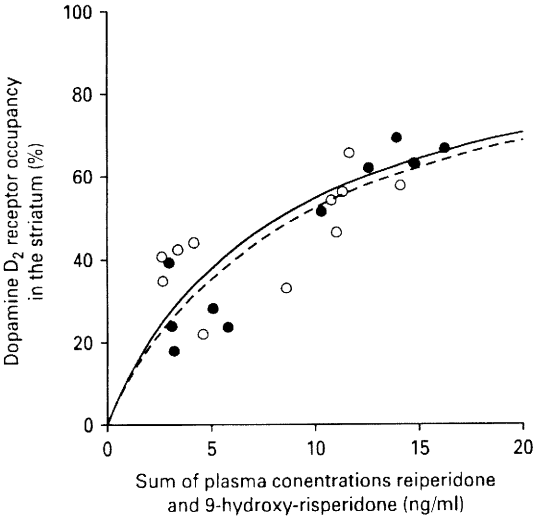

Fig. 2. The relationship between dopamine D_2 receptor occupancy in the striatum and the sum of plasma concentrations of risperidone and 9-hydroxy-risperidone. Open symbols (●) and solid curve (—) indicate receptor occupancy with [^{11}C]MNPA and its fitting curve, and solid symbols (○) and dashed curve (– – –) indicate receptor occupancy with [^{11}C]raclopride and its fitting curve, respectively. ED_{50} in the striatum was 8.32 ng/ml and 9.15 ng/ml for [^{11}C]MNPA and [^{11}C]raclopride, respectively.

Discussion

The present study demonstrated dopamine D_2R occupancies by risperidone measured with both [^{11}C]MNPA and [^{11}C]raclopride, i.e. the effects of risperidone on $D_{2,high}$ and $D_{2,low}$. The dopamine D_2R occupancies and ED_{50} values measured by [^{11}C]raclopride under risperidone administration were in agreement with most previous studies (Kapur *et al.* 1999; Nyberg *et al.* 1999;

Yasuno *et al.* 2001). In addition, the dose–occupancy curves and ED_{50} values with [^{11}C]MNPA were almost identical to those of [^{11}C]raclopride. Therefore, these results indicate that risperidone binds to both $D_{2,high}$ and $D_{2,low}$ at almost identical proportions. This is in accord with the report that risperidone is an antagonist for dopamine D_2Rs (Leysen *et al.* 1994) and has equal binding affinity to both $D_{2,high}$ and $D_{2,low}$ receptors (Seneca *et al.* 2006).

The [^{11}C]MNPA PET studies began 2 h after the start of the [^{11}C]raclopride PET studies. The sums of the plasma concentrations of risperidone and 9-hydroxyrisperidone were thus slightly higher during [^{11}C]raclopride studies (9.37 ± 4.89 ng/ml) than during [^{11}C]MNPA studies (7.74 ± 3.91 ng/ml), raising the possibility that the occupancy of [^{11}C]MNPA by dose could be underestimated in the present study. However, the ED_{50} value calculated by plasma concentrations showed almost identical values with the ED_{50} value by dose.

With regard to the *in-vivo* proportion of $D_{2,high}$ to $D_{2,low}$ in dopamine D_2Rs, several arguments have been put forward. Seneca *et al.* (2006) demonstrated that the sensitivity of striatal uptake of [^{11}C]MNPA is greater than that of [^{11}C]raclopride in response to amphetamine-induced dopamine release. It was indicated that [^{11}C]MNPA BP_{ND} was ~50% more sensitive to change than [^{11}C]raclopride to amphetamine-induced increase in synaptic dopamine. These authors suggested that 61% of the D_2Rs are configured in the high-affinity state (10% occupied by dopamine at baseline, 23% synaptic and 28% extrasynaptic) (Seneca *et al.* 2006). Narendran *et al.* (2010) also observed greater [^{11}C]NPA BP_{ND} reduction in response to amphetamine-induced dopamine release compared to [^{11}C]raclopride in healthy humans (Narendran *et al.* 2010). Moreover, Seeman (2009) demonstrated in their *ex-vivo* study that the dopamine agonist NPA inhibited [^{3}H]PHNO binding more than [^{3}H]raclopride did in amphetamine-sensitized rodents, indicating *in-vivo* competition of NPA to $D_{2,high}$ (Seeman, 2009). These experimental observations might provide psychopharmacological basis of dopamine D_2R hypersensitivity in patients with schizophrenia, i.e. use of psychostimulants worsens psychotic symptoms in patients with schizophrenia (Curran *et al.* 2004; Lieberman *et al.* 1987).

In contrast, Finnema *et al.* (2009) did not find distinguishable ID_{50} and K_i values of apomorphine for dopamine D_2Rs when measured with [^{11}C]MNPA and [^{11}C]raclopride (Finnema *et al.* 2009). *In-vitro* binding studies demonstrated that apomorphine binds to $D_{2,high}$ with 30- to 60-fold higher affinity compared to $D_{2,low}$ (De Lean *et al.* 1982; Sibley *et al.* 1982), and they suggest that almost all dopamine D_2Rs are in a high-affinity state at *in-vivo* condition. These findings might be the case for dopamine D_2 antagonists, partial as well as full agonists. Peng *et al.* (2010) found no significant differences of dopamine D_2R occupancy with [^{3}H]raclopride, [^{3}H]MNPA and [^{3}H]PHNO by using quinpirole (full agonist), aripiprazole (partial agonist), and haloperidol (antagonist) (Peng *et al.* 2010). A similar finding was observed in a previous *ex-vivo* study with [^{11}C]PHNO (McCormick *et al.* 2008). In clinical investigations, there is no clear evidence for the $D_{2,high}$ to $D_{2,low}$ proportion in dopamine D_2Rs. While ~20% differences of dopamine D_2R occupancy between [^{11}C]MNPA and [^{11}C]raclopride were observed in long-term treated patients with schizophrenia by Graff-Guerrero *et al.* (2009*a*), they found no significant differences of [^{11}C]PHNO binding in patients with schizophrenia-spectrum disorder amidst an acute psychotic episode group compared to control group (Graff-Guerrero *et al.* 2009*b*). In any case, further *in-vivo* investigations would be needed to elucidate the plausible ratio of $D_{2,high}$ to $D_{2,low}$. In particular, an *in-vivo* human receptor occupancy PET study using dopamine full agonists and/or partial agonists (e.g. an antipsychotic agent aripiprazole; Mamo *et al.* 2007) might help elucidate the $D_{2,high}$ and $D_{2,low}$ proportions in dopamine D_2Rs.

It is reported that a part of dopamine D_2R agonist radioligands shows higher affinity for dopamine D_3Rs. [^{11}C]PHNO is assumed to have ~50-fold higher selectivity to dopamine D_3Rs than to dopamine D_2Rs (Freedman *et al.* 1994; Narendran *et al.* 2006). This indicates that the observed differences of K_i value between [^{11}C]PHNO and [^{11}C]raclopride could be interpreted as the difference between D_2 and D_3 binding property. Meanwhile, a previous *ex-vivo* study showed that [^{11}C]MNPA has almost identical affinity to dopamine D_2 and D_3 receptors [2.21 nM (D_2) and 2.02 nM (D_3)] (Skinbjerg *et al.* 2009).

The dopamine D_2 antagonist administered could bind to dopamine D_2 autoreceptors as well as to post-synaptic dopamine D_2Rs. Blockade of dopamine D_2 autoreceptors could regulate dopaminergic neurotransmission in the present study. A recent human PET study on acute administration of the dopamine D_2 antagonist (risperidone) showed a stabilizing effect of risperidone on dopamine synthesis (Ito *et al.* 2009*b*). That study raised the possibility that acute administration of dopamine D_2R antagonist affects post-synaptic receptors by regulating the dopaminergic neurotransmission. Further study will be needed to elucidate the effect on dopamine D_2 autoreceptors.

In conclusion, dopamine D_2R occupancies by administration of risperidone, a dopamine D_2R antagonist, were measured in healthy subjects using both [^{11}C]raclopride and [^{11}C]MNPA. Almost identical occupancies were observed with the two radioligands, implying that risperidone binds to $D_{2,high}$ and $D_{2,low}$ at almost identical proportions in a dose-dependent manner. The present results of dose–occupancy curves with both radioligands also suggest that the same therapeutic window could be applicable to $D_{2,high}$ and for dopamine D_2Rs including both $D_{2,high}$ and $D_{2,low}$.

Acknowledgments

This study was supported in part by a Grant-in-Aid for the Molecular Imaging Program from the Ministry of Education, Culture, Sports, Science and Technology (MEXT). We thank Mr Katsuyuki Tanimoto and Mr Takahiro Shiraishi for their assistance in performing the PET experiments at the National Institute of Radiological Sciences. We also thank Ms. Yoshiko Fukushima of the National Institute of Radiological Sciences for her help as clinical research coordinator.

Statement of Interest

None.

References

Brix G, Zaers J, Adam LE, Bellemann ME, *et al.* (1997). Performance evaluation of a whole-body PET scanner using the NEMA protocol. National Electrical Manufacturers Association. *Journal of Nuclear Medicine* **38**, 1614–1623.

Curran C, Byrappa N, McBride A (2004). Stimulant psychosis: systematic review. *British Journal of Psychiatry* **185**, 196–204.

De Lean A, Kilpatrick BF, Caron MG (1982). Dopamine receptor of the porcine anterior pituitary gland. Evidence for two affinity states discriminated by both agonists and antagonists. *Molecular Pharmacology* **22**, 290–297.

Finnema SJ, Halldin C, Bang-Andersen B, Gulyas B, *et al.* (2009). Dopamine D(2/3) receptor occupancy of apomorphine in the nonhuman primate brain – a comparative PET study with [^{11}C]raclopride and [^{11}C]MNPA. *Synapse* **63**, 378–389.

Finnema SJ, Seneca N, Farde L, Shchukin E, *et al.* (2005). A preliminary PET evaluation of the new dopamine D_2 receptor agonist [^{11}C]MNPA in cynomolgus monkey. *Nuclear Medicine and Biology* **32**, 353–360.

Freedman SB, Patel S, Marwood R, Emms F, *et al.* (1994). Expression and pharmacological characterization of the human D3 dopamine receptor. *Journal of Pharmacology and Experimental Therapeutics* **268**, 417–426.

Gao YG, Baldessarini RJ, Kula NS, Neumeyer JL (1990). Synthesis and dopamine receptor affinities of enantiomers of 2-substituted apomorphines and their N-n-propyl analogues. *Journal of Medicinal Chemistry* **33**, 1800–1805.

George SR, Watanabe M, Di Paolo T, Falardeau P, *et al.* (1985). The functional state of the dopamine receptor in the anterior pituitary is in the high affinity form. *Endocrinology* **117**, 690–697.

Graff-Guerrero A, Mamo D, Shammi CM, Mizrahi R, *et al.* (2009*a*). The effect of antipsychotics on the high-affinity state of D2 and D3 receptors: a positron emission tomography study With [^{11}C]-(+)-PHNO. *Archives of General Psychiatry* **66**, 606–615.

Graff-Guerrero A, Mizrahi R, Agid O, Marcon H, *et al.* (2009*b*). The dopamine D2 receptors in high-affinity state and D3 receptors in schizophrenia: a clinical [^{11}C]-(+)-PHNO PET study. *Neuropsychopharmacology* **34**, 1078–1086.

Hwang DR, Kegeles LS, Laruelle M (2000). (−)-N-[(11)C]propyl-norapomorphine: a positron-labeled dopamine agonist for PET imaging of D(2) receptors. *Nuclear Medicine and Biology* **27**, 533–539.

Innis RB, Cunningham VJ, Delforge J, Fujita M, *et al.* (2007). Consensus nomenclature for in vivo imaging of reversibly binding radioligands. *Journal of Cerebral Blood Flow and Metabolism* **27**, 1533–1539.

Ito H, Arakawa R, Takahashi H, Takano H, *et al.* (2009*a*). No regional difference in dopamine D_2 receptor occupancy by the second-generation antipsychotic drug risperidone in humans: a positron emission tomography study. *International Journal of Neuropsychopharmacology* **12**, 667–675.

Ito H, Takano H, Takahashi H, Arakawa R, *et al.* (2009*b*). Effects of the antipsychotic risperidone on dopamine synthesis in human brain measured by positron emission tomography with L-[beta-^{11}C]DOPA: a stabilizing effect for dopaminergic neurotransmission? *Journal of Neuroscience* **29**, 13730–13734.

Kapur S, Zipursky RB, Remington G (1999). Clinical and theoretical implications of 5-HT2 and D2 receptor occupancy of clozapine, risperidone, and olanzapine in schizophrenia. *American Journal of Psychiatry* **156**, 286–293.

Lammertsma AA, Hume SP (1996). Simplified reference tissue model for PET receptor studies. *Neuroimage* **4**, 153–158.

Leysen JE, Janssen PM, Megens AA, Schotte A (1994). Risperidone: a novel antipsychotic with balanced serotonin-dopamine antagonism, receptor occupancy profile, and pharmacologic activity. *Journal of Clinical Psychiatry* **55**, 5–12.

Lieberman JA, Kane JM, Alvir J (1987). Provocative tests with psychostimulant drugs in schizophrenia. *Psychopharmacology* **91**, 415–433.

Mamo D, Graff A, Mizrahi R, Shammi CM, *et al.* (2007). Differential effects of aripiprazole on D(2), 5-HT(2), and 5-HT(1A) receptor occupancy in patients with schizophrenia: a triple tracer PET study. *American Journal of Psychiatry*, **164**, 1411–1417.

McCormick PN, Kapur S, Seeman P, Wilson AA (2008). Dopamine D2 receptor radiotracers [(11)C](+)-PHNO and [(3)H]raclopride are indistinguishably inhibited by D2 agonists and antagonists ex vivo. *Nuclear Medicine and Biology* **35**, 11–17.

Narendran R, Mason NS, Laymon CM, Lopresti BJ, *et al.* (2010). A comparative evaluation of the dopamine D(2/3) agonist radiotracer [^{11}C](−)-N-propyl-norapomorphine and antagonist [^{11}C]raclopride to measure amphetamine-induced dopamine release in the human striatum. *Journal of Pharmacology and Experimental Therapeutics*, **333**, 533–539.

Narendran R, Slifstein M, Guillin O, Hwang Y, *et al.* (2006). Dopamine (D2/3) receptor agonist positron emission tomography radiotracer [^{11}C]-(+)-PHNO is a D3 receptor preferring agonist in vivo. *Synapse* **60**, 485–495.

Neumeyer JL, Gao YG, Kula NS, Baldessarini RJ (1990). Synthesis and dopamine receptor affinity of (R)-(−)-2-fluoro-N-n-propylnorapomorphine: a highly potent and selective dopamine D2 agonist. *Journal of Medicinal Chemistry* **33**, 3122–3124.

Nyberg S, Eriksson B, Oxenstierna G, Halldin C, *et al.* (1999). Suggested minimal effective dose of risperidone based on PET-measured D2 and 5-HT2A receptor occupancy in schizophrenic patients. *American Journal of Psychiatry* **156**, 869–875.

Otsuka T, Ito H, Halldin C, Takahashi H, *et al.* (2009). Quantitative PET analysis of the dopamine D_2 receptor agonist radioligand ^{11}C-(R)-2-CH3O-N-n-propylnorapomorphine in the human brain. *Journal of Nuclear Medicine* **50**, 703–710.

Peng T, Zysk J, Dorff P, Elmore CS, *et al.* (2010). D2 receptor occupancy in conscious rat brain is not significantly distinguished with [(3)H]-MNPA, [(3)H]-(+)-PHNO, and [(3)H]-raclopride. *Synapse* **64**, 624–633.

Richfield EK, Penney JB, Young AB (1989). Anatomical and affinity state comparisons between dopamine D1 and D2 receptors in the rat central nervous system. *Neuroscience* **30**, 767–777.

Seeman P (2009). Dopamine D2 high receptors measured ex vivo are elevated in amphetamine-sensitized animals. *Synapse* **63**, 186–192.

Seeman P, Chau-Wong M, Tedesco J, Wong K (1975). Brain receptors for antipsychotic drugs and dopamine: direct binding assays. *Proceedings of the National Academy of Sciences USA* **72**, 4376–4380.

Seeman P, Weinshenker D, Quirion R, Srivastava LK, *et al.* (2005). Dopamine supersensitivity correlates with D_2 high states, implying many paths to psychosis. *Proceedings of the National Academy of Sciences USA* **102**, 3513–3518.

Seneca N, Finnema SJ, Farde L, Gulyas B, *et al.* (2006). Effect of amphetamine on dopamine D2 receptor binding in nonhuman primate brain: a comparison of the agonist radioligand [^{11}C]MNPA and antagonist [^{11}C]raclopride. *Synapse* **59**, 260–269.

Sibley DR, De Lean A, Creese I (1982). Anterior pituitary dopamine receptors. Demonstration of interconvertible high and low affinity states of the D-2 dopamine receptor. *Journal of Biological Chemistry* **257**, 6351–6361.

Skinbjerg M, Namkung Y, Halldin C, Innis RB, *et al.* (2009). Pharmacological characterization of 2-methoxy-N-propylnorapomorphine's interactions with D2 and D3 dopamine receptors. *Synapse* **63**, 462–475.

Suhara T, Sudo Y, Okauchi T, Maeda J, *et al.* (1999). Extrastriatal dopamine D_2 receptor density and affinity in the human brain measured by 3D PET. *International Journal of Neuropsychopharmacology* **2**, 73–82.

Takano A, Suhara T, Ikoma Y, Yasuno F, *et al.* (2004). Estimation of the time-course of dopamine D_2 receptor occupancy in living human brain from plasma pharmacokinetics of antipsychotics. *International Journal of Neuropsychopharmacology* **7**, 19–26.

Takano A, Suhara T, Yasuno F, Suzuki K, *et al.* (2006). The antipsychotic sultopride is overdosed: a PET study of drug-induced receptor occupancy in comparison with sulpiride. *International Journal of Neuropsychopharmacology* **9**, 539–545.

Watson C, Newport D, Casey M (1996). A single scatter simulation technique for scatter correction in 3D PET. In: Grangeat P, Amans JL (Eds), *Three-Dimensional Image Reconstruction in Radiology and Nuclear Medicine* (pp. 255–268). Dordrecht: Kluwer Academic Publishers.

Wilson AA, McCormick P, Kapur S, Willeit M, *et al.* (2005). Radiosynthesis and evaluation of [^{11}C]-(+)-4-propyl-3,4,4a,5,6,10b-hexahydro-2H-naphtho[1,2-b][1,4]oxazin-9-ol as a potential radiotracer for in vivo imaging of the dopamine D2 high-affinity state with positron emission tomography. *Journal of Medicinal Chemistry* **48**, 4153–4160.

Yasuno F, Suhara T, Okubo Y, Sudo Y, *et al.* (2001). Dose relationship of limbic-cortical D2-dopamine receptor occupancy with risperidone. *Psychopharmacology* **154**, 112–114.

NeuroImage 49 (2010) 578–586

Contents lists available at ScienceDirect

NeuroImage

journal homepage: www.elsevier.com/locate/ynimg

A new graphic plot analysis for determination of neuroreceptor binding in positron emission tomography studies

Hiroshi Ito [a,*], Takashi Yokoi [b], Yoko Ikoma [c], Miho Shidahara [c], Chie Seki [c], Mika Naganawa [c], Hidehiko Takahashi [a], Harumasa Takano [a], Yuichi Kimura [c], Masanori Ichise [d], Tetsuya Suhara [a]

[a] Clinical Neuroimaging Team, Molecular Neuroimaging Group, Molecular Imaging Center, National Institute of Radiological Sciences, 4-9-1 Anagawa, Inage-ku, Chiba 263-8555, Japan
[b] Bioimaging Laboratory, Inc., Kyoto, Japan
[c] Image Analysis Team, Biophysics Group, Molecular Imaging Center, National Institute of Radiological Sciences, Chiba, Japan
[d] Kreitchman PET Center, Department of Radiology, Columbia University College of Physicians, New York, NY, USA

ARTICLE INFO

Article history:
Received 27 March 2009
Revised 25 June 2009
Accepted 14 July 2009
Available online 23 July 2009

ABSTRACT

In positron emission tomography (PET) studies with radioligands for neuroreceptors, tracer kinetics have been described by the standard two-tissue compartment model that includes the compartments of nondisplaceable binding and specific binding to receptors. In the present study, we have developed a new graphic plot analysis to determine the total distribution volume (V_T) and nondisplaceable distribution volume (V_{ND}) independently, and therefore the binding potential (BP_{ND}). In this plot, $Y(t)$ is the ratio of brain tissue activity to time-integrated arterial input function, and $X(t)$ is the ratio of time-integrated brain tissue activity to time-integrated arterial input function. The x-intercept of linear regression of the plots for early phase represents V_{ND}, and the x-intercept of linear regression of the plots for delayed phase after the equilibrium time represents V_T. BP_{ND} can be calculated by $BP_{ND} = V_T / V_{ND} - 1$. Dynamic PET scanning with measurement of arterial input function was performed on six healthy men after intravenous rapid bolus injection of [^{11}C]FLB457. The plot yielded a curve in regions with specific binding while it yielded a straight line through all plot data in regions with no specific binding. V_{ND}, V_T, and BP_{ND} values calculated by the present method were in good agreement with those by conventional non-linear least-squares fitting procedure. This method can be used to distinguish graphically whether the radioligand binding includes specific binding or not.

Introduction

In positron emission tomography (PET) studies with radioligands for neuroreceptors, tracer kinetics have been described by the standard two-tissue compartment model containing the compartments of nondisplaceable binding and specific binding to receptors (Huang et al., 1986; Mintun et al., 1984). Based on the use of a radioligand with high specific radioactivity, the kinetic parameters can be determined by non-linear curve fitting procedure in a least-squares sense. To estimate the binding to receptors, the binding potential corresponding to specific binding to receptors and the total distribution volume including that of nondisplaceable and specific bindings are calculated from the kinetic parameters. To determine the total distribution volume, a graphic plot analysis developed by Logan et al. (1990) has also been used. By this method, only the total distribution volume can be calculated by simple linear least-squares fitting with rapid calculation time. This method can also be used to distinguish graphically whether the radioligand binding is reversible or not.

Previously, we developed a graphic plot analysis to determine cerebral blood flow and distribution volume with single-photon emission computed tomography and iodine-123-labeled N-isopropyl-4-iodoamphetamine, in which the tracer kinetics were determined according to the one-tissue compartment model (Yokoi et al., 1993). In that plot, $Y(t)$ is the ratio of brain tissue activity to time-integrated arterial input function, and $X(t)$ is the ratio of time-integrated brain tissue activity to time-integrated arterial input function. The y-intercept of linear regression of the plots represents cerebral blood flow, and the x-intercept represents the distribution volume. By this method, parameters can be rapidly calculated by simple linear least-squares fitting. However, this method has not been applied to PET studies with other radioligands in which the kinetics can be described by two-tissue compartment model.

In the present study, we applied our graphic plot analysis to the PET data of [^{11}C]FLB457, a radioligand for extrastriatal dopamine D_2 receptors. Using this method, the total distribution volume and nondisplaceable distribution volume corresponding to nondisplaceable binding could be determined independently by simple linear least-squares fitting, and as a result the binding potential could be calculated.

* Corresponding author. Fax: +81 43 253 0396.
E-mail address: hito@nirs.go.jp (H. Ito).

1053-8119/$ – see front matter © 2009 Elsevier Inc. All rights reserved.
doi:10.1016/j.neuroimage.2009.07.021

Materials and methods

Subjects

The study was approved by the Ethics and Radiation Safety Committees of the National Institute of Radiological Sciences, Chiba, Japan. Six healthy men (20–30 years of age) were recruited and their written informed consent was obtained. The subjects were healthy, based on their medical history of somatic or psychiatric disorders and magnetic resonance (MR) imaging of the brain.

PET procedures

PET studies were performed with a Siemens ECAT Exact HR+ system, which provides 63 sections with an axial field of view of 15.5 cm (Brix et al., 1997). The intrinsic spatial resolution was 4.3 mm in-plane and 4.2 mm full-width at half maximum (FWHM) axially. With a Hanning filter (cutoff frequency: 0.4 cycle/pixel), the reconstructed in-plane resolution was 7.5 mm FWHM. Data were acquired in three-dimensional mode. Scatter was corrected (Watson et al., 1996). A head fixation device with thermoplastic attachments for individual fit minimized head movement during PET measurements. A 10-min transmission scan using a ^{68}Ge–^{68}Ga line source was performed for correction of attenuation. After intravenous rapid bolus injection of [^{11}C]FLB457, data were acquired for 90 min in a consecutive series of time frames. The frame sequence consisted of nine 20-sec frames, five 1-min frames, four 2-min frames, eleven 4-min frames, and six 5-min frames. [^{11}C]FLB457 was synthesized as described previously (Halldin et al., 1995a; Suzuki et al., 1999b). The specific radioactivity of [^{11}C]FLB457 was 85–362 GBq/μmol at the time of injection. The radioactivity injected was 136–253 MBq.

To obtain the arterial input function, samples of arterial blood were taken periodically, twenty-eight in total. The fraction of radioactivity representing unchanged [^{11}C]FLB457 in plasma was determined by HPLC (Halldin et al., 1995b; Suzuki et al., 1999a; Swahn et al., 1994). For HPLC analysis, arterial blood samples were drawn at 3.5, 9, 18, 28, 39, 49, 59, 69, 79, and 89 min after injection. Plasma protein binding was not determined in the present study. The radioactivity of unchanged [^{11}C]FLB457 in plasma was used as the arterial input function.

Regions-of-interest

Regions-of-interest (ROIs) were drawn on the reconstructed PET images. ROIs were defined for the cerebellar cortex, thalamus, and four neocortical regions representing the frontal, temporal, parietal, and occipital lobes. Several circular ROIs, 8 mm in diameter, were located for each region covering 5–15 adjacent sections, and data were pooled to obtain the average radioactivity concentration for the whole volume of interest. To obtain regional time–activity curves, regional radioactivity was calculated for each frame, corrected for decay, and plotted versus time. To diminish the influence of tracer remaining in the blood, a standard value for regional cerebral blood volume (4%) and the curve for measured radioactivity in arterial whole blood were used. The thereby calculated radioactivity in the blood was then subtracted from the regional time–activity curves (Lammertsma et al., 1996).

Kinetic model

The time–activity curves of several neuroreceptor ligands with high specific radioactivity have been described by the standard two-tissue compartment model with four first-order rate constants (Fig. 1) (Huang et al., 1986; Mintun et al., 1984). Three compartments are defined. C_P is the radioactivity concentration of unchanged radioligand in plasma (arterial input function); C_{ND} is the radioactivity concentration of nondisplaceable radioligand in brain, which includes nonspecifically bound and free radioligand concentrations; C_S is the radioactivity concentration of radioligand specifically bound to receptors. The rate constants K_1 and k_2 describe the influx and efflux rates for radioligand diffusion through the blood brain barrier, respectively. The rate constants k_3 and k_4 describe the radioligand transfer between the compartments for nondisplaceable radioligand and specific radioligand binding to receptors. This model can be described by the following equations:

$$\frac{dC_{ND}(t)}{dt} = K_1 C_P(t) - (k_2 + k_3) C_{ND}(t) + k_4 C_S(t) \quad (1)$$

$$\frac{dC_S(t)}{dt} = k_3 C_{ND}(t) - k_4 C_S(t) \quad (2)$$

$$C_T(t) = C_{ND}(t) + C_S(t). \quad (3)$$

C_T is the total radioactivity concentration in a brain region as measured by PET.

A quantitative approach has been to express radioligand binding in terms of distribution volume concepts (Laruelle et al., 1994). Two such volumes expressed relative to the radioactivity concentration of unchanged radioligand in plasma (C_P) are defined by the following equations:

$$V_{ND} = \frac{K_1}{k_2} \quad (4)$$

$$V_T = \frac{K_1}{k_2}\left(1 + \frac{k_3}{k_4}\right). \quad (5)$$

V_{ND} is the distribution volume in a brain region with nondisplaceable binding only and thus is devoid of specific binding sites. V_T is the total distribution volume. Binding potential relative to the radioactivity concentration of nondisplaceable radioligand in brain (BP_{ND}), which reflects the ratio of receptor density (B_{max}) and affinity (K_D), is expressed as follows (Huang et al., 1986; Mintun et al., 1984):

$$BP_{ND} = \frac{k_3}{k_4} = \frac{V_T - V_{ND}}{V_{ND}}. \quad (6)$$

The time–activity curves of neuroreceptor ligands have also been described by the one-tissue compartment model with two rate constants (Ito et al., 1996; Koeppe et al., 1991) (Fig. 1). The rate constants K_i and k_o describe the influx and efflux rates for radioligand

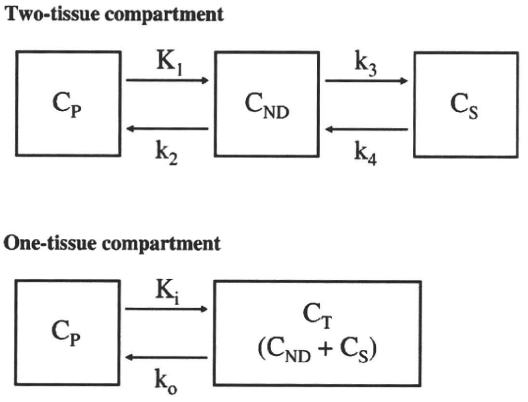

Fig. 1. Kinetic models to describe the time–activity curves of neuroreceptor ligands.

diffusion through the blood brain barrier, respectively. This model can be described by the following equation:

$$\frac{dC_T(t)}{dt} = K_i C_P(t) - k_o C_T(t). \quad (7)$$

In this model, V_T is defined as follows:

$$V_T = \frac{K_i}{k_o}. \quad (8)$$

Theory of graphic plot analysis

The integration of Eqs. (1) and (2) gives the following equations:

$$C_{ND}(t) = K_1 \int_0^t C_P(\tau)d\tau - (k_2 + k_3) \int_0^t C_{ND}(\tau)d\tau + k_4 \int_0^t C_S(\tau)d\tau \quad (9)$$

$$C_S(t) = k_3 \int_0^t C_{ND}(\tau)d\tau - k_4 \int_0^t C_S(\tau)d\tau. \quad (10)$$

Adding Eqs. (9) and (10) provides:

$$C_T(t) = K_1 \int_0^t C_P(\tau)d\tau - k_2 \int_0^t C_{ND}(\tau)d\tau. \quad (11)$$

By dividing both sides of Eq. 11 by $\int_0^t C_P(\tau)d\tau$, the following linear relationship is obtained:

$$\frac{C_T(t)}{\int_0^t C_P(\tau)d\tau} = K_1 - k_2 \frac{\int_0^t C_{ND}(\tau)d\tau}{\int_0^t C_P(\tau)d\tau}. \quad (12)$$

When $t \to 0$, C_T can be considered equal to C_{ND}.

$$Y(t) = K_1 - k_2 X(t) \quad (t \to 0) \quad (13)$$

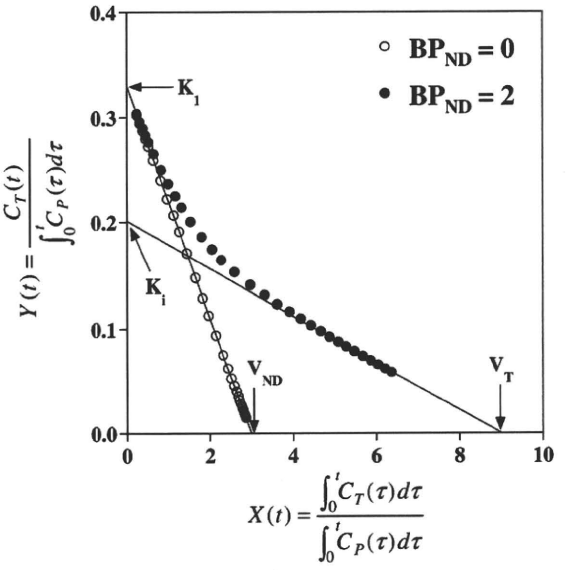

Fig. 2. An illustration of the present graphic plot analysis. When $t \to 0$, the y- and x-intercepts of the regression line represent K_1 and V_{ND}, respectively. When $t > t^*$ (t^*: equilibrium time), the x-intercept of the regression line represents V_T.

where

$$X(t) = \frac{\int_0^t C_T(\tau)d\tau}{\int_0^t C_P(\tau)d\tau}$$

$$Y(t) = \frac{C_T(t)}{\int_0^t C_P(\tau)d\tau}.$$

The plot of $Y(t)$ against $X(t)$ yields a straight line with a slope of $-k_2$ and a y-intercept equal to K_1 when $t \to 0$. Therefore, the x-intercept of the line represents V_{ND} (Fig. 2).

The integration of Eq. (7) gives the following equation:

$$C_T(t) = K_i \int_0^t C_P(\tau)d\tau - k_o \int_0^t C_T(\tau)d\tau. \quad (14)$$

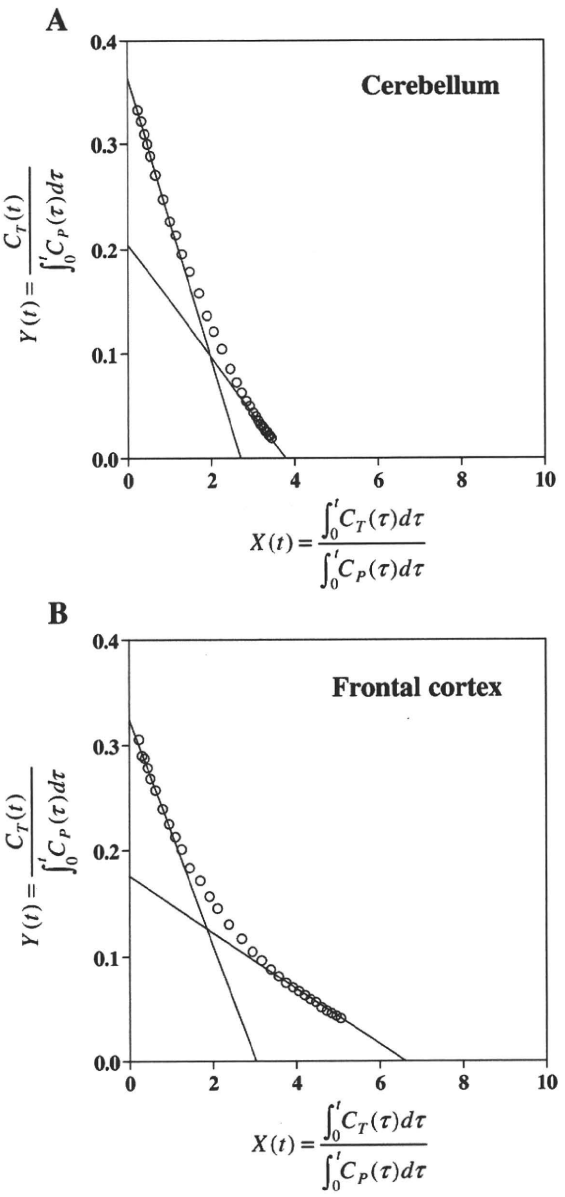

Fig. 3. Typical plots using the present graphic analysis in the cerebellum (A) and frontal cortex (B).

Table 1
Parameters calculated by kinetic analysis and the total distribution volume calculated by Logan plot analysis.

	Kinetic analysis							Logan plot analysis
	K_1 (mL/cm^3/min)	k_2 (min^{-1})	k_3 (min^{-1})	k_4 (min^{-1})	V_{ND} (mL/cm^3)	BP_{ND}	V_T (mL/cm^3)	V_T (mL/cm^3)
Cerebellum	0.360 ± 0.043	0.125 ± 0.007	0.018 ± 0.004	0.062 ± 0.030	2.88 ± 0.31	0.33 ± 0.14	3.85 ± 0.69	3.82 ± 0.62
Thalamus	0.354 ± 0.033	0.100 ± 0.025	0.123 ± 0.037	0.031 ± 0.004	3.66 ± 0.72	3.97 ± 0.72	18.01 ± 3.28	16.68 ± 1.91
Frontal cortex	0.345 ± 0.031	0.125 ± 0.021	0.071 ± 0.022	0.044 ± 0.007	2.79 ± 0.35	1.61 ± 0.37	7.29 ± 1.37	7.38 ± 1.29
Temporal cortex	0.316 ± 0.038	0.113 ± 0.027	0.110 ± 0.031	0.038 ± 0.005	2.87 ± 0.45	2.92 ± 0.69	11.20 ± 2.50	11.33 ± 2.26
Parietal cortex	0.331 ± 0.021	0.126 ± 0.023	0.080 ± 0.022	0.041 ± 0.007	2.70 ± 0.42	1.94 ± 0.32	7.94 ± 1.57	8.06 ± 1.50
Occipital cortex	0.330 ± 0.036	0.123 ± 0.018	0.052 ± 0.018	0.041 ± 0.008	2.73 ± 0.43	1.25 ± 0.23	6.14 ± 1.11	6.22 ± 1.10

Values are mean ± SD.

By dividing both sides of Eq. (14) by $\int_0^t C_P(\tau)d\tau$, the following linear relationship is obtained:

$$Y(t) = K_i - k_o X(t) \quad \left(t > t^*\right) \tag{15}$$

where

$$X(t) = \frac{\int_0^t C_T(\tau)d\tau}{\int_0^t C_P(\tau)d\tau}$$

$$Y(t) = \frac{C_T(t)}{\int_0^t C_P(\tau)d\tau}.$$

t^* is the equilibrium time. When $t \to \infty$, $X(t)$ equals V_T (Lassen, 1992). Therefore, the plot of $Y(t)$ against $X(t)$ reaches the x-intercept representing V_T with a slope of $-k_o$ and a y-intercept for K_i after the equilibrium time (Fig. 2) (see Appendix). When BP_{ND} is zero, the plot of $Y(t)$ against $X(t)$ yields a straight line with a slope of $-k_2$, a y-intercept of K_1 and an x-intercept of V_{ND} through all plot data (Fig. 2) (Yokoi et al., 1993).

In the measured PET data, plot data for early phase, from 90 to 330 s at mid-scan time, were used for linear least-squares fitting to calculate K_1 and V_{ND}, and plot data for delayed phase, from 62.5 to 87.5 min, which could be considered as being after the equilibrium time, were used for linear least-squares fitting to calculate V_T. The plot data from 10 to 70 s were not used because of noise due to short scan duration of each frame.

Kinetic analysis

To estimate the rate constants (K_1, k_2, k_3, and k_4) in the two-tissue compartment model for measured PET data, a conventional non-linear least-squares fitting procedure was also applied to the regional time–activity curves (Marquardt, 1963).

Logan plot analysis

The total distribution volume V_T was also calculated using the graphic plot analysis developed by Logan et al. (1990). In this analysis, plot data from 62.5 to 87.5 min were used for linear least-squares fitting to calculate V_T.

Simulation study

To estimate errors of K_1, V_{ND}, V_T, and BP_{ND}, a simulation study was performed. Tissue time–activity curves (0–90 min) for brain regions were generated according to the two-tissue compartment model. We assumed that the value for K_1 equaled 0.33 mL/cm^3/min, V_{ND} equaled 3.0 mL/cm^3 and k_4 equaled 0.04 min^{-1}. The tissue time–activity curves were generated with k_3 values between 0 and 0.2 min^{-1} in eleven steps. These assumed values were taken from the results obtained by kinetic analysis. The average of arterial input functions for all subjects was used for generating tissue time–activity curves. K_1, V_{ND}, V_T, and BP_{ND} values were calculated by the graphic plot analysis with these generated tissue time–activity curves, and were compared with the assumed values. In the graphic plot analysis, plot data from 90 to 330 s at mid-scan time were used to calculate K_1 and V_{ND}. Plot data from 62.5 to 87.5 min were used to calculate V_T.

Tissue time–activity curves with several noise levels were also generated to investigate the bias and variation of parameter estimates caused by statistical noise for the graphic plot analysis. The noise was generated with random numbers based on Gaussian distribution and added to the non-decaying tissue time–activity curves described above. The noise ratio for each time frame was determined according to the collected total count given by

$$\mathrm{NOISE}_i(\%) = \frac{\sqrt{N_i}}{N_i} \cdot 100 \tag{16}$$

$$N_i = \int_{t_i - \frac{\Delta t_i}{2}}^{t_i + \frac{\Delta t_i}{2}} C_T(t) \cdot e^{-\lambda t} \mathrm{dt} \cdot F \tag{17}$$

where i is the frame number, C_T is the non-decaying tissue radioactivity concentration derived from the rate constants and the arterial input function, t_i is the midpoint time of the i-th frame, Δt_i is the data collection time, λ is the radioisotope decay constant, and F is a scaling factor representing the sensitivity of the measurement system and is introduced here to adjust the noise level (Ikoma et al., 2008). The level of noise for the dynamic data was expressed as the mean of percent noise described in Eq. (16) from 1.5 to 90 min. In this simulation study, F was chosen so that the mean of percent noise would be 1%, 3%, 5%, 7%, and 10%, and a thousand noisy data sets were generated for each. In these noise-added tissue time–activity curves, V_{ND}, V_T, and BP_{ND} values were calculated by the present graphic plot analysis. V_T was also calculated using the Logan plot analysis. Reliability of the estimated parameters was evaluated by the bias of median and quartile deviation of the estimates.

Results

Typical plots using the present graphic analysis are shown in Fig. 3. Using the present plot analysis, K_1, V_{ND}, V_T, and BP_{ND} values could be calculated rapidly by linear least-squares fitting. The K_1, V_{ND}, V_T, and

Table 2
Parameters calculated by the present graphic plot analysis.

	K_1 (mL/cm^3/min)	V_{ND} (mL/cm^3)	BP_{ND}	V_T (mL/cm^3)
Cerebellum	0.371 ± 0.050	2.82 ± 0.37	0.36 ± 0.08	3.85 ± 0.64
Thalamus	0.349 ± 0.028	4.40 ± 0.57	3.16 ± 0.75	18.04 ± 1.85
Frontal cortex	0.340 ± 0.025	3.17 ± 0.36	1.32 ± 0.20	7.40 ± 1.29
Temporal cortex	0.312 ± 0.030	3.40 ± 0.47	2.32 ± 0.35	11.35 ± 2.25
Parietal cortex	0.326 ± 0.019	3.13 ± 0.44	1.57 ± 0.21	8.07 ± 1.50
Occipital cortex	0.328 ± 0.035	2.97 ± 0.41	1.09 ± 0.14	6.23 ± 1.10

Values are mean ± SD.

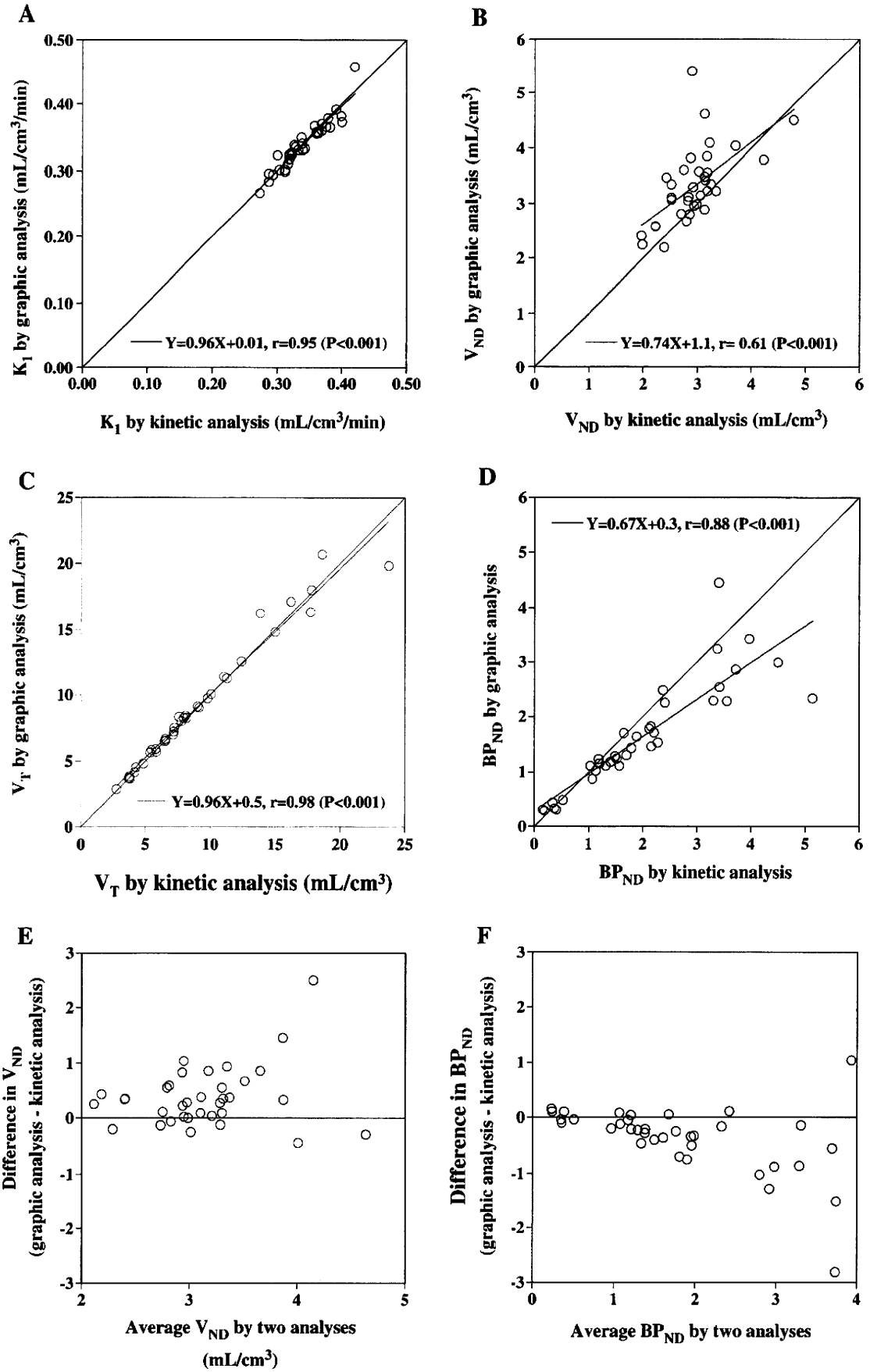

Fig. 4. Relations between kinetic analysis and graphic plot analysis in K_1 (A), V_{ND} (B), V_T (C), and BP_{ND} (D). The Bland–Altman plots for V_{ND} (E) and BP_{ND} (F) are also shown.

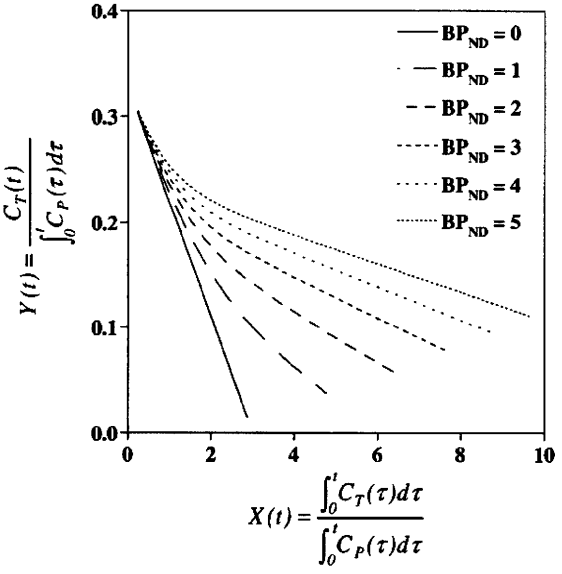

Fig. 5. Simulation of graphic plots for BP_{ND} of 0 to 5.

BP_{ND} values calculated by kinetic analysis and the present graphic plot analysis are shown in Tables 1 and 2. Overestimation of V_{ND} and underestimation of BP_{ND} by the graphic plot analysis were prominent in regions with high BP_{ND}. The coefficients of variation were almost the same between the two analytical methods. The relations between kinetic analysis and graphic plot analysis in K_1, V_{ND}, V_T, and BP_{ND} are shown in Fig. 4. Good correlations were observed in all parameters. The Bland–Altman plots for V_{ND} and BP_{ND} are also shown in Fig. 4. V_T values were in good agreement between Logan plot analysis and the present graphic plot analysis (Tables 1 and 2).

Simulated graphic plots are shown in Fig. 5. The plot yields a curve in regions with specific binding. The plot for delayed phase shows an approximate straight line, which can be considered as being after the equilibrium time. In regions with no specific binding, the plot yields a straight line through all plot data. Errors in K_1, V_{ND}, V_T, and BP_{ND} values calculated by graphic plot analysis were simulated in Fig. 6. Systemic overestimation of V_{ND} and underestimation of BP_{ND} by graphic plot analysis were observed. When the assumed BP_{ND} was greater, the magnitudes of the systemic overestimation and underestimation were greater.

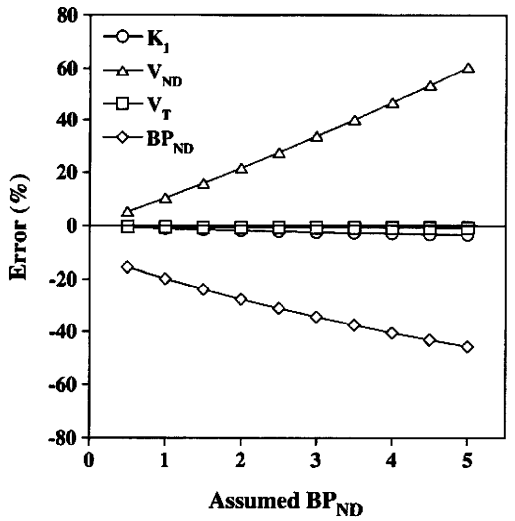

Fig. 6. Errors in K_1, V_{ND}, V_T, and BP_{ND} by graphic plot analysis estimated with simulated tissue time–activity curves.

The bias of median and quartile deviation of V_{ND}, V_T, and BP_{ND} estimated by simulation studies with noise-added tissue time–activity curves are shown in Figs. 7 and 8. The quartile deviations of V_{ND} and BP_{ND} became larger as the noise level increased, while the bias was almost constant. V_T calculated by Logan plot analysis was underestimated when the noise level was high whereas the bias of V_T calculated by the present graphic plot analysis was negligibly small. On the other hand, the quartile deviation of V_T by the present graphic plot analysis was larger than that by Logan plot analysis when the noise level was high.

Discussion

In the present graphic plot analysis, the plot yields a curve in regions with specific binding for both measured and simulated data while it yields a straight line through all plot data in regions with no specific binding. This indicates that the present analysis can be used to distinguish graphically whether the radioligand binding includes specific binding or not. In this study, the plot yields a curve for the cerebellum. Although specific [^{11}C]FLB457 binding in the cerebellum was not supported statistically in previous studies (Olsson et al., 1999; Suhara et al., 1999), it has recently been reported that a non-negligible

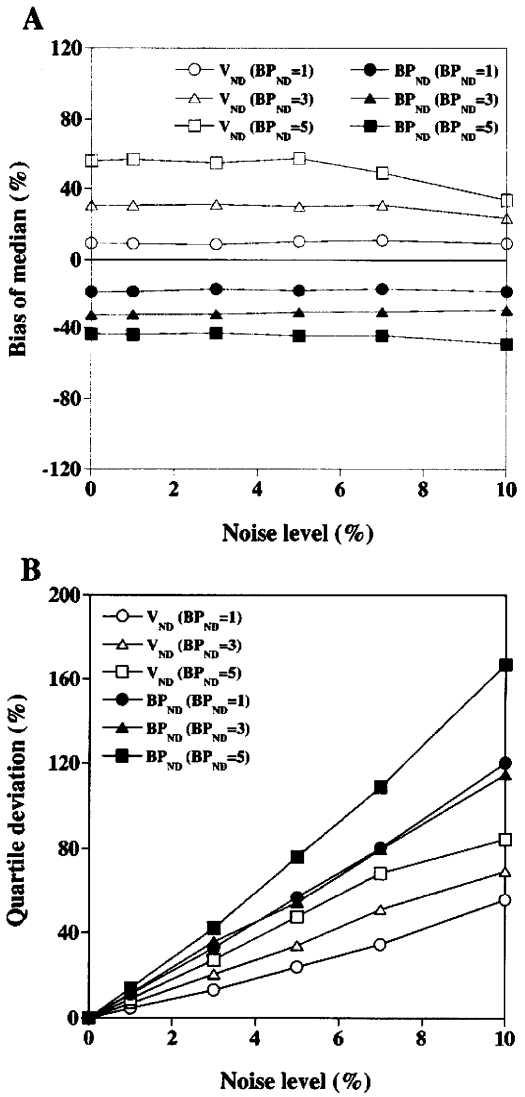

Fig. 7. The bias of median (A) and quartile deviation (B) of V_{ND} and BP_{ND} by the graphic plot analysis estimated with noise-added tissue time–activity curves.

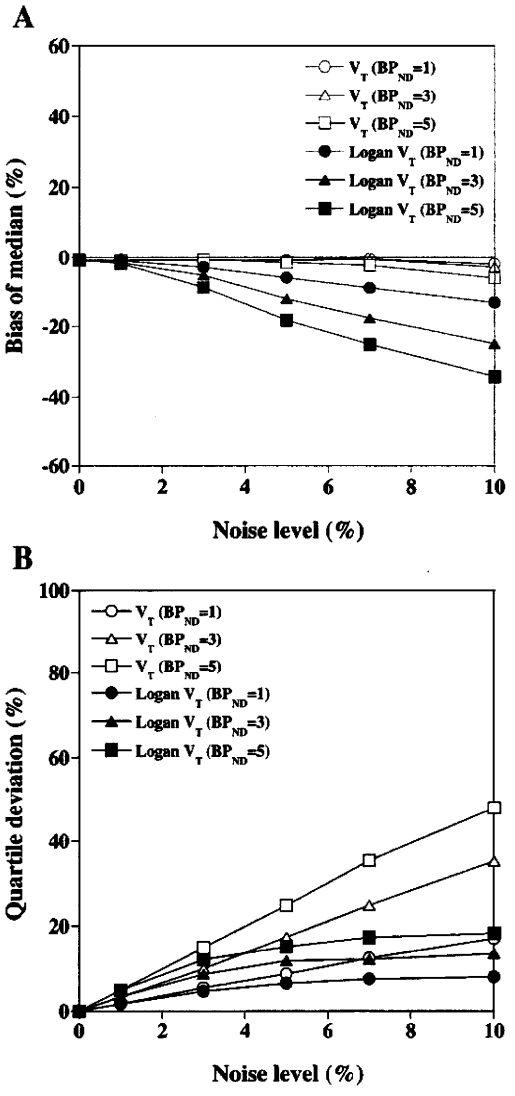

Fig. 8. The bias of median (A) and quartile deviation (B) of V_T by the present graphic plot analysis and Logan plot analysis estimated with noise-added tissue time–activity curves.

density of dopamine D_2 receptors in the cerebellum led to the underestimation of BP_{ND} in a brain region in [^{11}C]FLB457 PET studies when the cerebellum was used as a reference brain region for calculation of BP_{ND} (Asselin et al., 2007). A curve plot for the cerebellum can indicate a non-negligible density of dopamine D_2 receptors in this region. Although the present graphic plot analysis was applied to [^{11}C]FLB457 that showed relatively high affinity to dopamine D_2 receptors in this study, this graphic plot analysis can also be applied to other radioligands with low affinity, e.g., [^{11}C]raclopride in order to distinguish whether the radioligand binding includes specific binding or not.

Specific binding to receptors can be estimated by kinetic analysis with a non-linear least-squares fitting procedure based on the standard two-tissue compartment model containing compartments of nondisplaceable binding and specific binding. However, a non-linear least-squares fitting procedure is time-consuming and the separation of nondisplaceable and specific binding is often made unstable by noisy time–activity data. In the present graphic plot analysis, the plot showed an approximate straight line after the equilibrium time, and both V_{ND} and V_T could be rapidly calculated independently by linear least-squares fitting. Although systemic overestimation of V_{ND}, and therefore systemic underestimation of BP_{ND}, was observed in the present graphic plot analysis, the K_1, V_{ND}, V_T, and BP_{ND} values were in good agreement between the kinetic analysis and the present graphic plot analysis, indicating its validity. In the present study, plot data for only early phase (90–330 s) were used to calculate V_{ND} by the present graphic plot analysis, and therefore estimation of V_{ND} might not be reliable. In simulation studies, the quartile deviation of V_{ND} became larger as the noise level increased. However, coefficients of variation of V_{ND} were almost the same between the kinetic analysis and the present graphic plot analysis. If earlier phase of PET data with reduced noise level can be used, the systemic errors in V_{ND} and BP_{ND} calculated by the present graphic plot analysis can be reduced.

Logan plot analysis could also reveal the V_T values with the linear least-squares fitting procedure, similar to the present graphic plot analysis. The V_T values were in good agreement between the two graphic plot analyses. In the present graphic plot analysis, linear regression of the plots for delayed phase would be horizontal for radioligands with irreversible binding (Yokoi et al., 1993). Thus, this graphic plot analysis can be used to distinguish the reversibility of radioligand binding graphically, as can Logan plot analysis. It has been reported that noise in time–activity data caused a bias in the V_T values in Logan plot analysis (Logan et al., 2001). In simulation studies, the bias of V_T calculated by the present graphic plot analysis was negligibly small whereas that by Logan plot analysis was larger as the noise level increased. However, the quartile deviation of V_T by the present graphic plot analysis was larger than that by Logan plot analysis when the noise level was high.

In this study, we applied the present graphic plot analysis to the standard two-tissue compartment model with four rate constants. In this regard, a three-tissue compartment model with six rate constants including k_5 and k_6, in which the compartment of nondisplaceable radioligand was divided into compartments of nonspecifically bound and free radioligand, has also been proposed to describe the kinetics of radioligands for neuroreceptors (Wong et al., 1986). To generalize the theory of this graphic plot analysis for multi-tissue compartment model, further studies will be required.

Using the present analysis, parametric maps of V_{ND}, V_T, and BP_{ND} can be calculated on a voxel-by-voxel basis in a rapid manner. Because the time–activity data in a voxel is noisy, the variations of V_{ND} and BP_{ND} calculated using the present analysis method might be large for parametric mapping. More caution should be given in calculation of parametric images. Recently, a method for the determination of input function without arterial blood sampling was developed (Naganawa et al., 2005). Using this method combined with the present graphic method, it may be possible to calculate a parametric map of BP_{ND} without arterial blood sampling and without the use of a reference brain region that has negligible specific binding.

In conclusion, we have applied a new graphic plot analysis to PET data of a radioligand for extrastriatal dopamine D_2 receptors. Using this method, V_{ND}, V_T, and BP_{ND} could be calculated with a rapid calculation time. The V_{ND}, V_T, and BP_{ND} values calculated by this method were in good agreement with those by conventional non-linear least-squares fitting procedure. This method can be used to distinguish graphically whether the radioligand binding includes specific binding or not. In addition, the reversibility of radioligand binding can also be distinguished graphically by this method.

Acknowledgments

This study was supported in part by a Grant-in-Aid for Molecular Imaging Program from the Ministry of Education, Culture, Sports, Science and Technology (MEXT), Japanese Government and a grant from the National Institute of Radiological Sciences. The assistance of members of the National Institute of Radiological Sciences staff in performing the PET experiments is also gratefully acknowledged.

Appendix

The time course of the radioactivity in multi-compartment systems driven by an arterial input function $C_P(t)$ can be expressed as follows (Logan et al., 1990; Patlak and Blasberg, 1985):

$$\frac{d}{dt}\mathbf{C_T} = \mathbf{K}\mathbf{C_T} + \mathbf{Q}C_P(t) \tag{A1}$$

where $\mathbf{C_T}$ is the column vector of radioactivity concentrations for each tissue compartment at time t, $\mathbf{K}$ is the matrix of rate constants, and $\mathbf{Q}$ is the vector describing the influx rate constant from plasma to brain. Eq. (A1) can be written as follows (Logan et al., 1990; Patlak and Blasberg, 1985):

$$\mathbf{U_n^T}\mathbf{K}^{-1}\mathbf{C_T} = \mathbf{U_n^T}\mathbf{K}^{-1}\mathbf{Q}\int_0^t C_P(\tau)d\tau + \int_0^t C_T(\tau)d\tau \tag{A2}$$

where $\mathbf{U_n^T}$ is a row vector of 1s and $C_T(t) = \mathbf{U_n^T}\mathbf{C_T}$. The total radioactivity in a region-of-interest, ROI(t), contains the intravascular radioactivity and is expressed as follows:

$$\mathrm{ROI}(t) = C_T(t) + V_P C_P(t) = \mathbf{U_n^T}\mathbf{C_T} + V_P C_P(t) \tag{A3}$$

where V_P is the plasma volume in a region-of-interest that depends on the first-pass extraction fraction of tracer. With Eq. (A3), Eq. (A2) becomes the following:

$$\begin{aligned}\frac{\mathrm{ROI}(t)}{\mathbf{U_n^T}\mathbf{C_T} + V_P C_P(t)} &= \mathbf{U_n^T}\mathbf{K}^{-1}\mathbf{C_T} \\ &= \left(\mathbf{U_n^T}\mathbf{K}^{-1}\mathbf{Q} - V_P\right)\int_0^t C_P(\tau)d\tau \\ &\quad + \int_0^t \mathrm{ROI}(\tau)d\tau.\end{aligned} \tag{A4}$$

By dividing both sides of Eq. (A4) by $\int_0^t C_P(\tau)d\tau$, the following linear relationship is obtained:

$$\begin{aligned}\frac{\mathrm{ROI}(t)}{\int_0^t C_P(\tau)d\tau} &= \frac{\mathbf{U_n^T}\mathbf{C_T} + V_P C_P(t)}{\mathbf{U_n^T}\mathbf{K}^{-1}\mathbf{C_T}}\left(\mathbf{U_n^T}\mathbf{K}^{-1}\mathbf{Q} - V_P\right) \\ &\quad + \frac{\mathbf{U_n^T}\mathbf{C_T} + V_P C_P(t)}{\mathbf{U_n^T}\mathbf{K}^{-1}\mathbf{C_T}}\frac{\int_0^t \mathrm{ROI}(\tau)d\tau}{\int_0^t C_P(\tau)d\tau}.\end{aligned} \tag{A5}$$

The relation $\mathbf{C_T} = -\mathbf{K}^{-1}\mathbf{Q}C_P(t)$ after the equilibrium time has been shown (steady-state condition) (Patlak et al., 1983), and Eq. (A5) becomes the following:

$$Y(t) = \frac{\left(-\mathbf{U_n^T}\mathbf{K}^{-1}\mathbf{Q} + V_P\right)^2}{\mathbf{U_n^T}\mathbf{K}^{-2}\mathbf{Q}} - \frac{-\mathbf{U_n^T}\mathbf{K}^{-1}\mathbf{Q} + V_P}{\mathbf{U_n^T}\mathbf{K}^{-2}\mathbf{Q}}X(t) \tag{A6}$$

where

$$X(t) = \frac{\int_0^t \mathrm{ROI}(\tau)d\tau}{\int_0^t C_P(\tau)d\tau}$$

$$Y(t) = \frac{\mathrm{ROI}(t)}{\int_0^t C_P(\tau)d\tau}.$$

Eq. (A6) is the generalized equation of the present graphic plot analysis. The plot of $Y(t)$ against $X(t)$ yields a straight line after the equilibrium time t^*. The slope, y-intercept, and x-intercept are follows:

$$\text{y-intercept} = \frac{\left(-\mathbf{U_n^T}\mathbf{K}^{-1}\mathbf{Q} + V_P\right)^2}{\mathbf{U_n^T}\mathbf{K}^{-2}\mathbf{Q}} \tag{A7}$$

$$\text{slope} = -\frac{-\mathbf{U_n^T}\mathbf{K}^{-1}\mathbf{Q} + V_P}{\mathbf{U_n^T}\mathbf{K}^{-2}\mathbf{Q}} \tag{A8}$$

$$\text{x-intercept} = -\mathbf{U_n^T}\mathbf{K}^{-1}\mathbf{Q} + V_P. \tag{A9}$$

When the two-tissue compartment model with four rate constants is applied (Fig. 1), the vectors are defined as follows:

$$\mathbf{U_n^T} = [1 \quad 1] \qquad \mathbf{C_T} = \begin{bmatrix} C_{ND}(t) \\ C_S(t) \end{bmatrix} \quad \mathbf{Q} = \begin{bmatrix} K_1 \\ 0 \end{bmatrix}$$

$$\mathbf{K} = \begin{bmatrix} -(k_2 + k_3) & k_4 \\ k_3 & -k_4 \end{bmatrix}.$$

With these vectors and neglecting V_P, the slope, y-intercept, and x-intercept are defined as follows:

$$\text{y-intercept}(K_i) = \frac{K_1}{1 + \frac{k_2 k_3}{(k_3 + k_4)^2}} \tag{A10}$$

$$\text{slope} = \frac{-k_2 k_4}{k_3 + k_4 + \frac{k_2 k_3}{k_3 + k_4}} \tag{A11}$$

$$\text{x-intercept} = \frac{K_1}{k_2}\left(1 + \frac{k_3}{k_4}\right). \tag{A12}$$

From Eqs. (4), (5), and (A10), k_3 and k_4 can be calculated as follows:

$$k_3 = \frac{K_1 K_i}{K_1 - K_i}\frac{(V_T - V_{ND})^2}{V_{ND} V_T^2} \tag{A13}$$

$$k_4 = \frac{K_1 K_i}{K_1 - K_i}\frac{V_T - V_{ND}}{V_T^2}. \tag{A14}$$

References

Asselin, M.C., Montgomery, A.J., Grasby, P.M., Hume, S.P., 2007. Quantification of PET studies with the very high-affinity dopamine D_2/D_3 receptor ligand [^{11}C]FLB 457: re-evaluation of the validity of using a cerebellar reference region. J. Cereb. Blood Flow Metab. 27, 378–392.

Brix, G., Zaers, J., Adam, L.E., Bellemann, M.E., Ostertag, H., Trojan, H., Haberkorn, U., Doll, J., Oberdorfer, F., Lorenz, W.J., 1997. Performance evaluation of a whole-body PET scanner using the NEMA protocol. J. Nucl. Med. 38, 1614–1623.

Halldin, C., Farde, L., Hogberg, T., Mohell, N., Hall, H., Suhara, T., Karlsson, P., Nakashima, Y., Swahn, C.G., 1995a. Carbon-11-FLB 457: a radioligand for extrastriatal D_2 dopamine receptors. J. Nucl. Med. 36, 1275–1281.

Halldin, C., Swahn, C.G., Farde, L., Sedvall, G., 1995b. Radioligand disposition and metabolism – key information in early drug development. In: Comer, D. (Ed.), PET for Drug Development and Evaluation. Kluwer Academic Publisher, The Netherlands, pp. 55–65.

Huang, S.C., Barrio, J.R., Phelps, M.E., 1986. Neuroreceptor assay with positron emission tomography: equilibrium versus dynamic approaches. J. Cereb. Blood Flow Metab. 6, 515–521.

Ikoma, Y., Ito, H., Arakawa, R., Okumura, M., Seki, C., Shidahara, M., Takahashi, H., Kimura, Y., Kanno, I., Suhara, T., 2008. Error analysis for PET measurement of dopamine D_2 receptor occupancy by antipsychotics with [^{11}C]raclopride and [^{11}C] FLB 457. NeuroImage 42, 1285–1294.

Ito, H., Goto, R., Koyama, M., Kawashima, R., Ono, S., Sato, K., Fukuda, H., 1996. A simple method for the quantification of benzodiazepine receptors using iodine-123 iomazenil and single-photon emission tomography. Eur. J. Nucl. Med. 23, 782–791.

Koeppe, R.A., Holthoff, V.A., Frey, K.A., Kilbourn, M.R., Kuhl, D.E., 1991. Compartmental analysis of [^{11}C]flumazenil kinetics for the estimation of ligand transport rate and receptor distribution using positron emission tomography. J. Cereb. Blood Flow Metab. 11, 735–744.

Lammertsma, A.A., Bench, C.J., Hume, S.P., Osman, S., Gunn, K., Brooks, D.J., Frackowiak, R.S., 1996. Comparison of methods for analysis of clinical [^{11}C]raclopride studies. J. Cereb. Blood Flow Metab. 16, 42–52.

Laruelle, M., Baldwin, R.M., Rattner, Z., al-Tikriti, M.S., Zea-Ponce, Y., Zoghbi, S.S., Charney, D.S., Price, J.C., Frost, J.J., Hoffer, P.B., Innis, R.B., 1994. SPECT quantification of [^{123}I]iomazenil binding to benzodiazepine receptors in nonhuman primates: I. Kinetic modeling of single bolus experiments. J. Cereb. Blood Flow Metab. 14, 439–452.

Lassen, N.A., 1992. Neuroreceptor quantitation in vivo by the steady-state principle using constant infusion or bolus injection of radioactive tracers. J. Cereb. Blood Flow Metab. 12, 709–716.

Logan, J., Fowler, J.S., Volkow, N.D., Wolf, A.P., Dewey, S.L., Schlyer, D.J., MacGregor, R.R., Hitzemann, R., Bendriem, B., Gatley, S.J., Christman, D.R., 1990. Graphical analysis of reversible radioligand binding from time–activity measurements applied to [N-^{11}C-methyl]-(−)-cocaine PET studies in human subjects. J. Cereb. Blood Flow Metab. 10, 740–747.

Logan, J., Fowler, J.S., Volkow, N.D., Ding, Y.S., Wang, G.J., Alexoff, D.L., 2001. A strategy for removing the bias in the graphical analysis method. J. Cereb. Blood Flow Metab. 21, 307–320.

Marquardt, D., 1963. An algorithm for least-squares estimation of nonlinear parameters. J. Soc. Indust. Appl. Math. 11, 431–441.

Mintun, M.A., Raichle, M.E., Kilbourn, M.R., Wooten, G.F., Welch, M.J., 1984. A quantitative model for the in vivo assessment of drug binding sites with positron emission tomography. Ann. Neurol. 15, 217–227.

Naganawa, M., Kimura, Y., Nariai, T., Ishii, K., Oda, K., Manabe, Y., Chihara, K., Ishiwata, K., 2005. Omission of serial arterial blood sampling in neuroreceptor imaging with independent component analysis. NeuroImage 26, 885–890.

Olsson, H., Halldin, C., Swahn, C.G., Farde, L., 1999. Quantification of [^{11}C]FLB 457 binding to extrastriatal dopamine receptors in the human brain. J. Cereb. Blood Flow Metab. 19, 1164–1173.

Patlak, C.S., Blasberg, R.G., 1985. Graphical evaluation of blood-to-brain transfer constants from multiple-time uptake data. Generalizations. J. Cereb. Blood Flow Metab. 5, 584–590.

Patlak, C.S., Blasberg, R.G., Fenstermacher, J.D., 1983. Graphical evaluation of blood-to-brain transfer constants from multiple-time uptake data. J. Cereb. Blood Flow Metab. 3, 1–7.

Suhara, T., Sudo, Y., Okauchi, T., Maeda, J., Kawabe, K., Suzuki, K., Okubo, Y., Nakashima, Y., Ito, H., Tanada, S., Halldin, C., Farde, L., 1999. Extrastriatal dopamine D_2 receptor density and affinity in the human brain measured by 3D PET. Int. J. Neuropsychopharmacol. 2, 73–82.

Suzuki, K., Takei, M., Kida, T., 1999a. Development of an analyzing system for the sensitive measurement of radioactive metabolites on the PET study. J. Labelled Compd Radiopharm. 42, S658–660.

Suzuki, K., Yamazaki, T., Sasaki, M., Kubodera, A., 1999b. Approach to ultra high specific activity for ^{11}C-labeled compounds — synthesis of [^{11}C]FLB-457 and [^{11}C]Ro15-4513. J. Labelled Compd Radiopharm. 42, S129–131.

Swahn, C.G., Halldin, C., Farde, L., Sedvall, G., 1994. Metabolism of the PET ligand [^{11}C] SCH23390. Identification of two radiolabelled metabolites with HPLC. Hum. Psychopharmacol. 9, 25–31.

Watson, C.C., Newport, D., Casey, M.E., 1996. A single scatter simulation technique for scatter correction in 3D PET. In: Grangeat, P., Amans, J.L. (Eds.), Three-Dimensional Image Reconstruction in Radiology and Nuclear Medicine. Kluwer Academic Publishers, The Netherlands, pp. 255–268.

Wong, D.F., Gjedde, A., Wagner Jr, H.N., 1986. Quantification of neuroreceptors in the living human brain. I. Irreversible binding of ligands. J. Cereb. Blood Flow Metab. 6, 137–146.

Yokoi, T., Iida, H., Itoh, H., Kanno, I., 1993. A new graphic plot analysis for cerebral blood flow and partition coefficient with iodine-123-iodoamphetamine and dynamic SPECT validation studies using oxygen-15-water and PET. J. Nucl. Med. 34, 498–505.